Palaeoproterozoic magnesite–stromatolite–dolostone–'red bed' association, Russian Karelia: palaeoenvironmental constraints on the 2.0 Ga-positive carbon isotope shift

VICTOR A. MELEZHIK, ANTHONY E. FALLICK, PAVEL V. MEDVEDEV & VLADIMIR V. MAKARIKHIN

Melezhik, V. A., Fallick, A. E., Medvedev, P. V. & Makarikhin, V. V.: Palaeoproterozoic magnesite–stromatolite–dolostone–'red bed' association, Russian Karelia: palaeoenvironmental constraints on the 2.0 Ga-positive carbon isotope shift. *Norsk Geologisk Tidsskrift,* Vol. 80, pp. 163–186. Oslo 2000. ISSN 0029-196X.

The ca. 2000 Mà Tulomozerskaya Formation, Russian Karelia, is composed of an 800 m-thick magnesite–stromatolite–dolostone–'red bed' succession with the most ^{13}C-rich dolostones (up to +18‰ V-PDB) that have ever been reported. Terrigenous 'red beds' are developed throughout the sequence and represent three main depositional settings: (1) a braided fluvial system over a lower energy, river-dominated coastal plain, (2) a low-energy, barred lagoon or bight, and (3) a non-marine, playa lake. A significant component of the sequence consists of biostromal and biohermal columnar stromatolites accreted in shallow-water, low-energy, intertidal zones, barred evaporitic lagoons and peritidal evaporitic environments. Only a small portion of stromatolites might have been accreted in relatively 'open' marine environments. The red, flat-laminated, dolomitic and magnesite stromatolites formed in evaporative ephemeral ponds, coastal sabkhas and playa lakes. Tepees, mudcracks, pseudomorphs after calcium sulphate, halite casts, and abundant 'red beds' in the sequence suggest that (1) terrestrial environments dominated over aqueous, and (2) partial or total decoupling took place between the stromatolite-dominated depositional systems and the bordering sea. The greatest enrichment in ^{13}C occurs in the playa magnesite (up to +17.2‰) and in the laminated dolomitic stromatolites accreted in ephemeral ponds (up to +16.8‰), whereas the dolostones from more open environments are less rich in ^{13}C (+5.6 to +10.7‰). The isotopic shift (ca. 5‰) induced by global factors (i.e. accelerated accumulation of organic material in an external basin) was augmented by that driven by a series of local factors (restriction, evaporation, biological photosynthesis). The latter enhanced a global $\delta^{13}C$ value due to an isotopic disequilibrium between atmospheric CO_2 and dissolved inorganic carbon in the local aquatic reservoirs precipitating the carbonate minerals. The interplay between global and local factors should be taken into account when interpreting the Palaeoproterozoic carbon isotope excursion and its implications.

Victor A. Melezhik, Geological Survey of Norway, Leiv Eirikssons vei 39, 7491 Trondheim, Norway; Anthony E. Fallick, Scottish Universities Environmental Research Centre, East Kilbride, Glasgow G75 0QF, Scotland, UK; Pavel V. Medvedev & Vladimir V. Makarikhin, Institute of Geology of Karelian Scientific Centre, Russian Academy of Sciences, Pushkinskaya, 11, 185610 Petrozavodsk, Russian Karelia, Russia

Introduction

Since the pioneering work of Schidlowski et al. (1976), the existence of unusually ^{13}C-rich dolostones in Africa deposited at around 2.3 Ga (the Lomagundi event) has puzzled geologists. While this so-called 'Lomagundi event' was ascribed to locally enhanced burial of organic matter in a restricted basin (Schidlowski et al. 1976), two additional discoveries of ca. 2.0 Ga-old calcite marbles with extremely positive $\delta^{13}C$ values led to a reassessment of this event as global in nature (Baker & Fallick 1989a, b). The carbon isotope excursion was interpreted as the result of an increase in the global fraction of carbon buried as organic matter.

However, despite the fact that the global significance of the high Palaeoproterozoic $\delta^{13}C$ values has recently been re-emphasized (Karhu & Holland 1996), the geological data necessary for understanding the mechanism responsible for $\delta^{13}C$ values as high as +10 to +18‰ are not yet available (Melezhik & Fallick 1996; Melezhik et al. 1999). The local carbonate $\delta^{13}C$ may consist of a global background value together with a regional signature dependent on the specific palaeoenvironmental setting; therefore, the true global background value of $\delta^{13}C$ for this period of time remains a subject for debate (Shields 1997; Melezhik & Fallick 1997), and our understanding of the carbon cycle is incomplete.

To date, most high $\delta^{13}C$ values reported for Palaeoproterozoic successions are based on material for which there is very limited information on depositional environments (e.g. Schidlowski et al. 1976; Baker & Fallick 1989a, b; Karhu 1993; Melezhik & Fallick 1996). Consequently, discrimination between global and local factors contributing to this excursion has not yet been made.

The focus of this article is a succession of stromatolitic dolostones, magnesite and terrigeneous 'red beds' represented by the ca. 2 billion-year-old Tulomozerskaya Formation (TF) in the Onega Lake area, Russian Karelia (Fig. 1). Ever since Yudovich et al. (1991) published $\delta^{13}C$ values up to +18‰, the Tulomozerskay dolostones have been the most ^{13}C-rich sedimentary carbonates ever reported (Melezhik et al. 1999), thus occupying an exceptional position in the Palaeoproterozoic high $\delta^{13}C$ records and calling for a detailed assessment of the

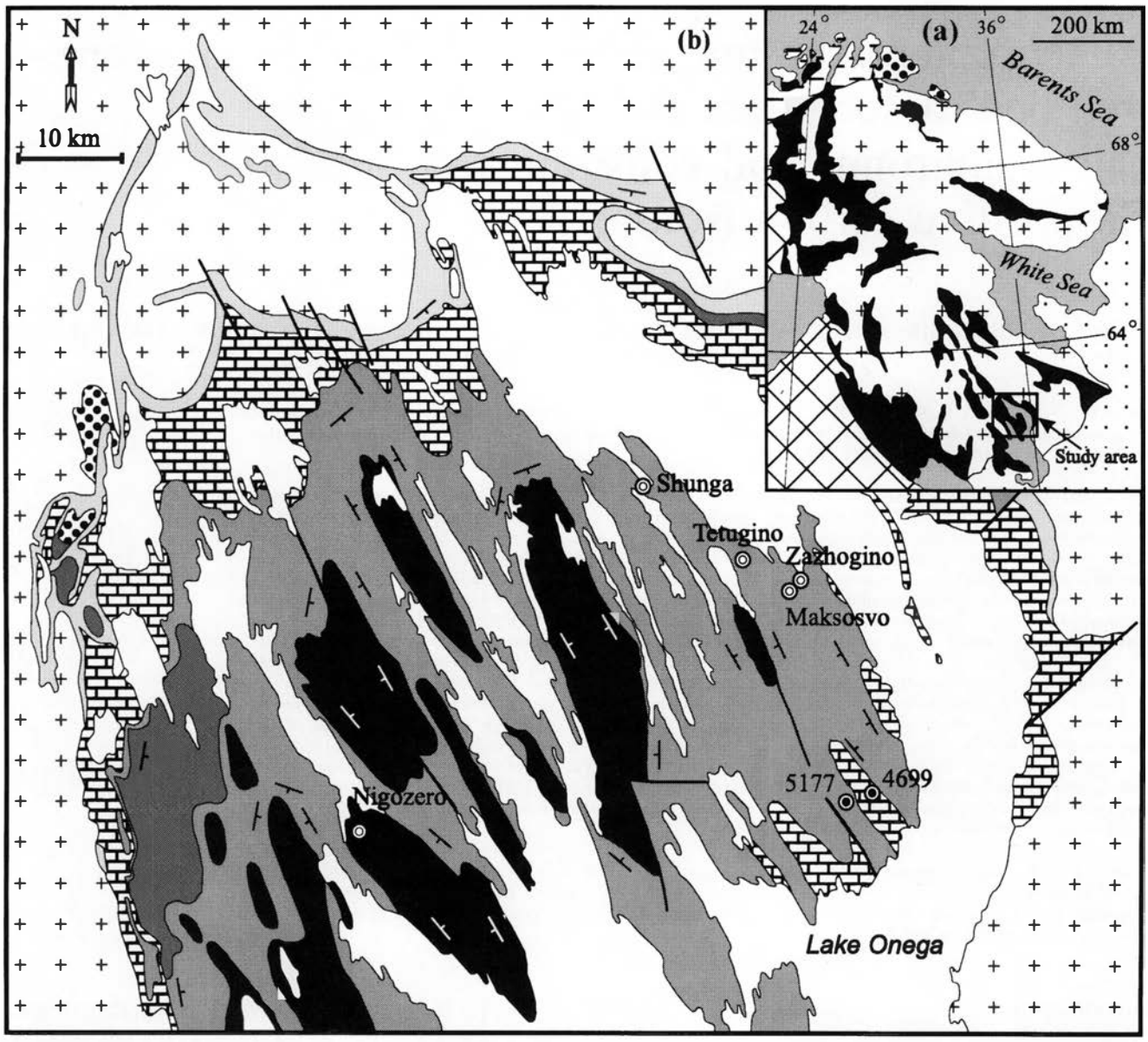

Fig. 1. (a, inset) Geographical and geological location of the study area, and (b) geological map of the northern Onega Lake area (simplified from Akhmedov et al. 1993).

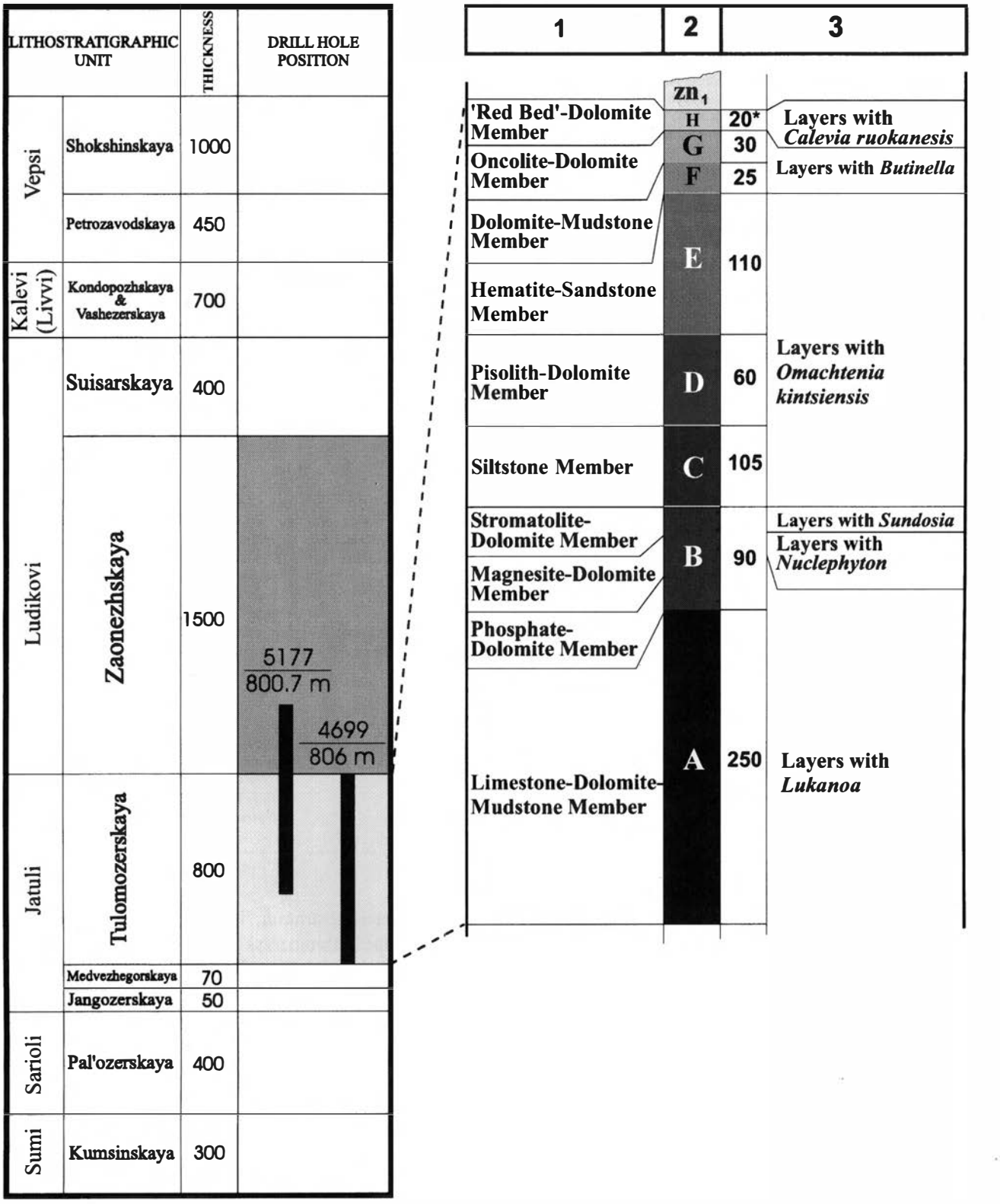

Fig. 2. Stratigraphic position of the studied drillholes and lithostratigraphical subdivisions of the northern Onega Lake area as suggested by: 1: Akhmedov et al. (1993), 2: present authors, 3: Makarikhin & Medvedev (cited in Akhmedov et al. 1993). The thickness is shown in metres as measured in drillholes 4699 (Member A) and 5177 (Members B, C, D, E, F, G and H). zn_1 is the Zaonezhskaya Formation.

palaeoenvironment. The formation was intensively drilled for the purpose of establishing and describing the Palaeoproterozoic stratotype of the Russian Federation. Consequently, drillcore material has become available enabling detailed sedimentological and palaeontological study.

Although detailed isotopic and geochemical data on the TF have been presented in Melezhik et al. (1999), this

Table 1. Interpreted depositional environments of the Tulomozerskaya Formation.

Member	Thickness, m	Lithofacies	Rock assemblage	Colour	Stromatolite morphology	Interpreted depositional environment
H	20	VII, X	Allochemical and stromatolitic dolostone	Red	Spaced, low-relief bioherms, flat-laminated stromatolites.	Swash zone frequently exposed to air (VII); intertidal (X).
G	30	X	Oncolitic and stromatolitic dolostone	Pink, brown	Very closely spaced bioherms, oncolites.	Intertidal–subtidal (X).
F	25	III, V	Siltstone, sandstone, stromatolitic dolostone, amygdaloidal basalt	Grey, pink	Flat-laminated stromatolites, oncolites.	Playa lake, ponded tidal flat (III); low-energy tidal zone in barred lagoon (V).
E	110	III, V, X	Quartz sandstone, siltstone with a carbonate matrix; three intervals of stromatolitic dolostone	Pink	Flat-laminated stromatolites.	Playa lake, ponded tidal flat (III); low-energy tidal zone in barred lagoon (V); playa lake (X).
D	60	IV, V, VIII, IX, X	Oncolitic and stromatolitic dolostone and magnesite, dolostone breccia, siltstone	Grey, pink	Oncolites; spaced, single, large columns; laterally continuous biostromes.	Low-energy intertidal zone in barred lagoon (IV); peritidal, evaporitic (V); playa lake, sabkha (VIII, IX); intertidal–subtidal (X).
B	90	I, VI, IX, X	Stromatolitic dolostone with 1–2 m thick magnesite band, quartz sandstone	Pale grey	Laterally continuous biostromes; spaced bioherms; spaced, single, large columns; oncolites; flat-laminated stromatolites.	Braided fluvial system over a low-energy, river-dominated, coastal plain (I); barred, evaporitic lagoon (VI); playa lake, sabkha (IX); a complex combination of intertidal (barred lagoon), shallow-water subtidal zones and ephemeral ponds in supratidal zone (X).
C	105	IV, V, VIII, X	Siltstone and sandstone intercalated with stromatolitic dolostone	Red	Laterally continuous biostromes; flat-laminated stromatolites; oncolites.	Low-energy intertidal zone in barred lagoon (IV); peritidal, evaporitic (V); playa lake, sabkha (VIII); a combination of intertidal zone in barred lagoon and ephemeral ponds in supratidal zone (X).
A	250	I, II, IV, V, VIII, IX, X	Stromatolitic dolostone alternating with quartz sandstone and siltstone, subordinate dolostone breccia	Pink	Flat-laminated stromatolites; markedly divergent, small, columnar stromatolites.	Braided fluvial system over a low-energy, river-dominated, coastal plain (I); upper-tidal, protected (II); low-energy intertidal zone in barred lagoon (IV); peritidal, evaporitic (V); playa lake, sabkha (VIII, IX); ephemeral ponds in supratidal zone (X).

contribution provides a sedimentological ground for the interpretation of ^{13}C-rich dolostones. Consequently, this paper should contribute to our understanding of both the depositional environments of ^{13}C-rich dolostones and the carbon cycle in the Palaeoproterozoic.

Geological background

The Palaeoproterozoic TF is preserved in a synform exposed on the northern coast of Lake Onega, as well as on its islands and peninsulas, occupying an area of 10,000 km^2 (Fig. 1). The Onega synform consists of a number of smaller NW-SE-trending and SE-plunging synforms and antiforms. The sequence of the Onega Lake area includes seven formations (Fig. 2), namely, the Pal'ozerskaya, Jangozerskaya, Medvezhegorskaya, Tulomozerskaya, Zaonezhskaya, Suisarskaya and Vashezerskaya formations (Sokolov 1987). The Palaeoproterozoic rocks, with the Pal'ozerskaya basal polymict conglomerates and diamictites, unconformably overlie the Archaean substratum. The Jangozerskaya, Medvezhegorskaya and Tulomozerskaya formations are collectively known as the Jatulian Group (Sokolov 1970, 1980; Negrutza 1984). The stratotype section of the Jatulian Group (Sokolov 1987) begins with the 50–120 m-thick Jangozersakaya Formation, which rests either conformably on the Pal'ozerskaya conglomerates or unconformably on weathered Archaean gneisses and granites. The Jangozersakaya strata comprise predominantly red, cross-bedded terrigenous rocks. These rocks are conformably overlain by the 70 m-thick Medvezhegorskaya Formation consisting of mafic lava with subordinate cross-bedded quartz sandstones, gritstones and 'red beds'. The TF conformably overlies the Medvezhegorskaya succession. The formation is described in detail in following sections.

The three Jatulian formations are unconformably overlain by C_{org}-rich siltstones and mudstones (shungite rocks) with subordinate dolostones of the 1500 m-thick Zaonezhskaya Formation. This is followed by the Suisarskaya Formation, a 400 m-thick succession of basalts intercalated with numerous gabbro sills. A gabbro intrusion from the

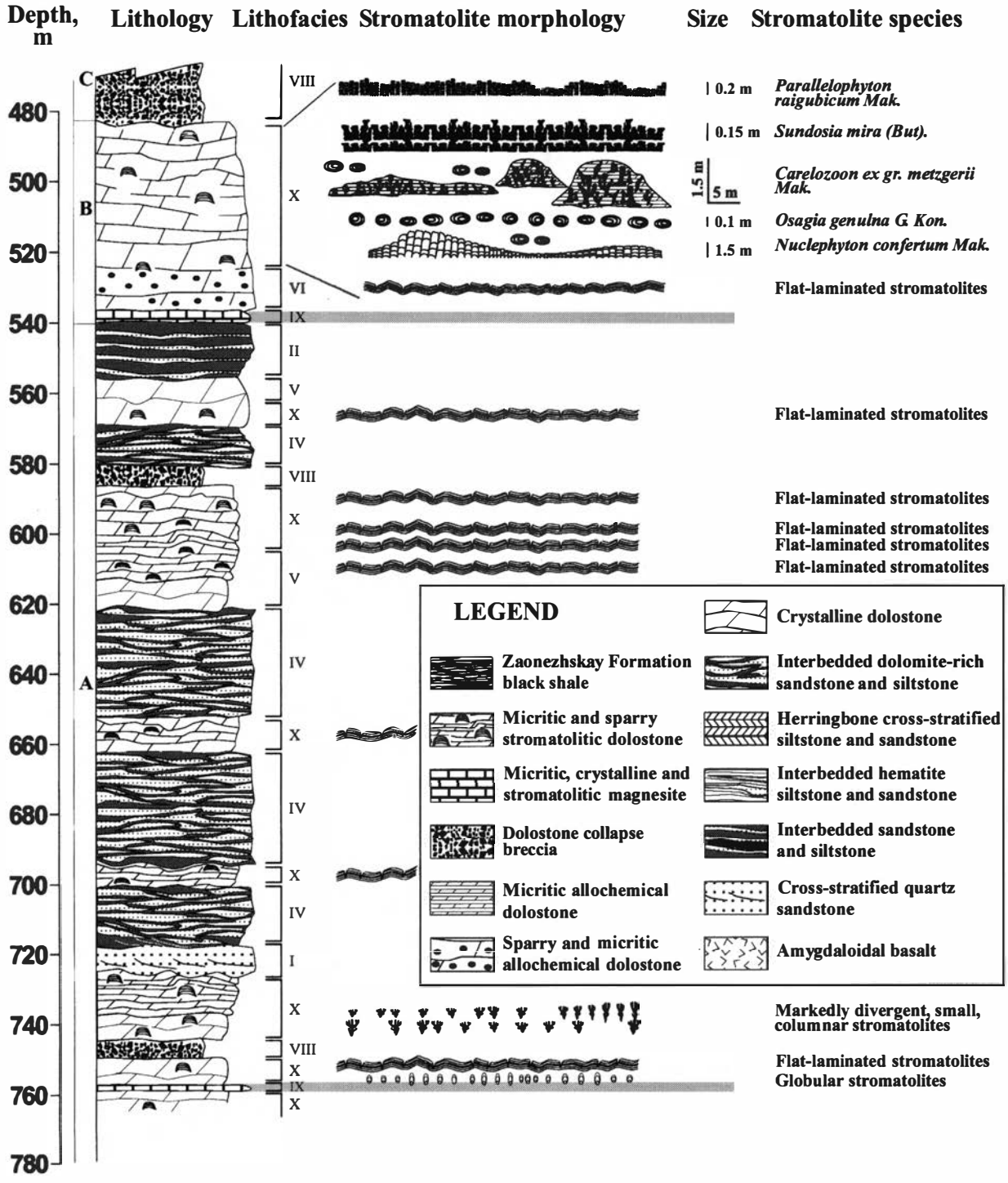

Fig. 3. The main stromatolite morphologies versus lithostratigraphy, drillhole 4699. Grey bars mark magnesite layers.

upper part of the Suisarskaya Formation has given a Sm-Nd mineral isochron age of 1980 ± 27 Ma (Pukhtel et al. 1992). The succession ends with the 190 m-thick Vashezerskaya Formation comprising greywacke and arkosic sandstones.

The Palaeoproterozoic rocks were deformed and underwent greenschist facies metamorphism during the 1.8 Ga Svecofennian orogeny. The paragenesis chlorite–actinolite–epidote reflects a temperature of 300–350°C.

Lithostratigraphical subdivision of the TF

The lithostratigraphic subdivision is based on drillcores. The drillholes studied, 5177 (35°25′00″E, 62°14′29″N) and 4699 (35°28′00″E, 62°14′30″N), were made by the Karelian Geological Expedition and intersect an 800 m-thick succession (Fig. 2) located north of Lake Onega (Fig. 1).

The TF has been divided into a number of 'piles'

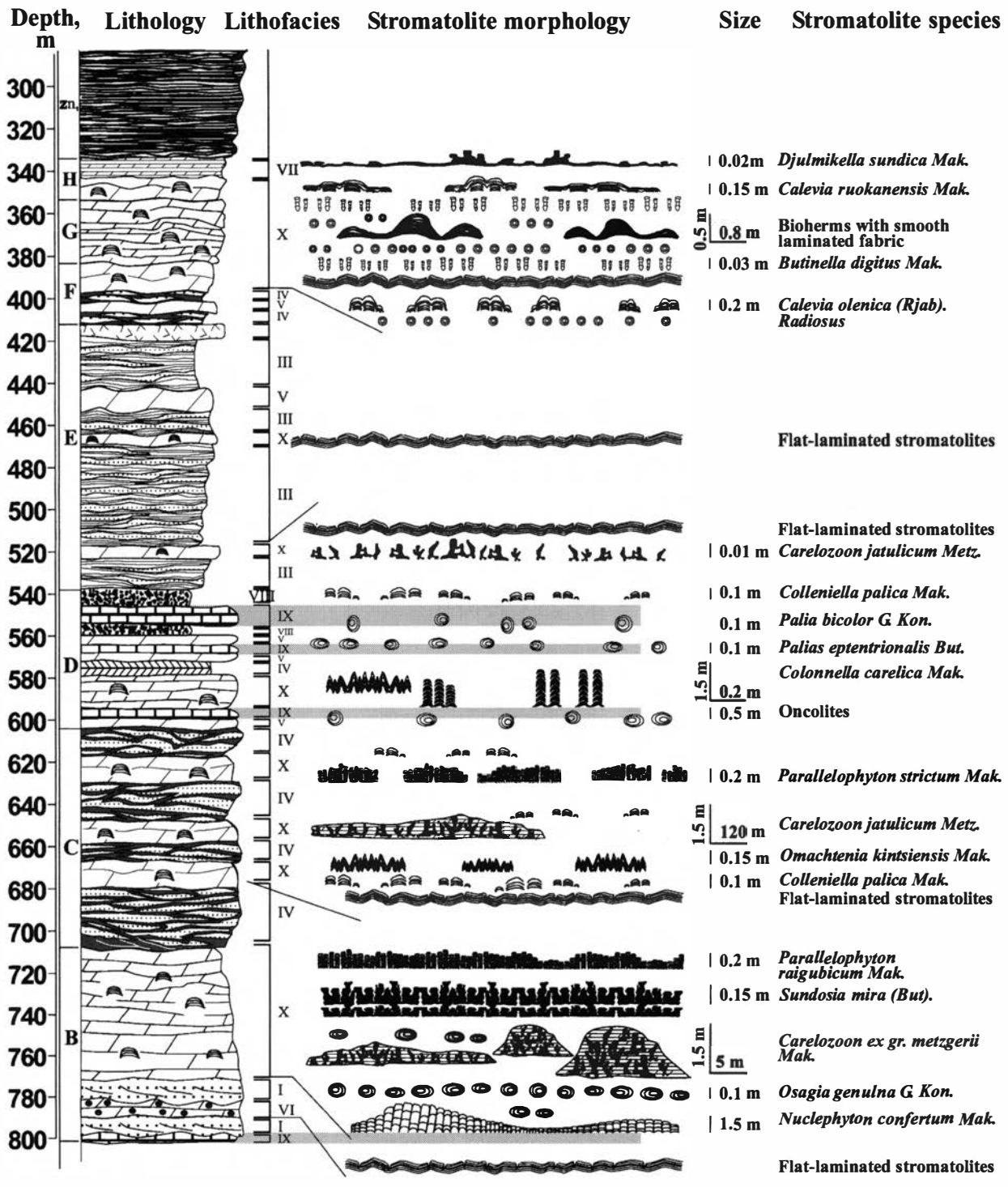

Fig. 4. The main stromatolite morphologies versus lithostratigraphy, drillhole 5177. Grey bars mark magnesite layers. For the legend, see Fig. 3.

(Akhmedov et al. 1993), renamed here as 'members' (Fig. 2) in accordance with the International Stratigraphic Code (ISSC 1976). For practical reasons and for consistency we have substituted letters for Russian names, starting with 'A' for the lowermost Limestone–Dolostone–Mudstone Member. The whole succession, consisting of eight lithostratigraphic members (A–H), can also be divided into six biostratigraphic units, each with distinctive stromatolites, oncolites and microfossils (Fig. 2). Principal features of the lithostratigraphic Members A to H are summarized in Table 1.

Lithofacies of the Tulomozerskaya Formation

Facies analysis is based on drillcore material supported by available outcrops in the area adjacent to the drilling site, which provide good information on structural features and

their spatial distribution. The main lithofacies recognized in the sequence are described below.

Lithofacies I consists of dolomite-bearing quartz sandstones which occur in the drillholes as 8–10 m-thick beds in the lower part of Members A and B (Figs. 3, 4), where they have an erosional base. The sandstones are reddish-grey to grey, ripple-marked, cross-stratified or structureless. Silty material has not been observed. Tabular sets of unidirectional, 1–3 cm-thick cross-stratification are common in Members A and B. Rare asymmetric ripples have low relief with amplitudes of 0.3–0.5 cm and wavelengths of 1–4 cm. The sandstone beds of Member A in places bear decimetre-scale channels filled with cross-bedded, fining-upward, coarse-grained sandstones. Northwest of the drilling site the Lithofacies I quartz sandstones may reach a thickness of 200 m. In such cases they comprise a fining-upward sequence, which starts with sheet-like bodies of variegated, rhythmically-bedded gritstones and coarse-grained sandstones grading upwards into medium- to fine-grained sandstones. The latter dominate and exhibit abundant unidirectional, trough and tabular cross-stratification (Sokolov et al. 1970; Heiskanen 1990). In places up to 2 m-wide and 0.5 m-deep erosional channels filled with coarser, fining-upward sand material have been observed (Heiskanen, pers. comm. 1999). Vertically accreting beds are less common.

Lithofacies II is a 20 m-thick unit of sandstones interbedded with siltstones and mudstones in the uppermost part of Member A. The sedimentary rocks are thin, parallel-bedded or lenticular-bedded. The lenticular bedding is expressed by the development of small lenses of sandstone in silty and muddy beds. An apparent lack of reworking leaves the beds intact.

Lithofacies III is recognized by intercalated brown, hematite mudstones, siltstones and pink quartz sandstones, which are only developed in Member E. Mature sandstones with dolomite cement are the dominant lithology forming 5–70 cm-thick, platy, cross-stratified beds. The siltstones are hematite-rich and marked by abundant desiccation cracks. The fine laminae of the siltstones characteristically define low-relief hummocks and swells with amplitudes of less than 1 cm and wavelengths of 1–3 cm. A 1–2 m-thick bed of clastic hematite ore and halite cube casts in red mudstones and siltstones has been reported from this lithofacies (Akhmedov et al. 1993). A 50 m-thick flow of amygdaloidal basalt has been observed in the uppermost part of Lithofacies III.

Lithofacies IV consists of grey, beige and pale pink, fine-grained, dolomite-rich sandstones, siltstones and mudstones. Many of the layers show distinctive herringbone cross-bedding and flaser bedding. Rhythms, 1–4 cm thick, consisting of sand and mud couplets, or cross-bedded sand layers and lenses between muddy material are characteristic. The Member A siltstones contain pseudomorphs after crystals of gypsum (Fig. 5a), which in places are distinguished by the 'swallow tail' twin morphology. Lithofacies IV has been recognized in Members A, C, D and F.

Lithofacies V is composed of variegated, structureless or indistinctly parallel-laminated dolostones. Micritic dolostones and marls of Members B, C and D are sporadically marked by desiccation cracks and by dolomite pseudomorphs after displacive, isolated, small crystals of gypsum (Akhmedov et al. 1993). Some of these pseudomorphs are distinguished by the 'swallow tail' twin morphology. The desiccation cracks are quartz sand-filled, several decimetre-scale in width and display 2–3 centimetre-scale penetration (Fig. 5b). Syndepositional deformation expressed as tepee structures is a common feature of Member C (Akhmedov et al. 1993).

Lithofacies VI is a red grainstone. The rocks are typically structureless (Fig. 5c) or crudely stratified by variations in colour and grain size. Dolarenite and dolorudite are very characteristic features of Member B, though they have also been observed in Member A. Members F and H contain beds of grainstones only in places. The limited number of grainstones (Figs. 3, 4) may be caused by a high degree of recrystallization. Allochems (0.1–8 mm) are represented by unsorted, both rounded and angular intraclasts of micritic and sparry dolostones. Other clasts are rounded quartz grains, sporadic hematite and siliceous oolites. Shaly laminae are very common. Cement, when preserved, is represented by a syntaxial dolomite spar overgrowth on micritic and sparry dolomite intraclasts (Fig. 6). These overgrowths are cloudy and rich in inclusions. Generally, burial syntaxial overgrowths are clear, whereas inclusion-rich and cloudy, syntaxial, dolomite spar is considered to represent earlier overgrowths (e.g. Tucker & Wright 1990, pp. 351–352). Clear, syntaxial, dolomite overgrowths, which apparently precipitated in the burial environment, have been documented only once. The matrix of sparry allochemical dolostones may be classified as either crystalline dolomite (Fig. 7a) or, to a lesser extent, mosaic dolomite spar; both are rich in gas/fluid inclusions (Fig. 7b). The latter may indicate that the matrix has undergone diagenetic alteration at low water/rock ratios (e.g. Carpenter & Lohman 1997). Abundant vugs, voids (filled with drusy dolomite) and cauliflower-like aggregates of quartz with crude radial fabric (Fig. 8a) are very characteristic features. The millimetre-scale aggregates of cauliflower-quartz are represented by two varieties. The first one, with castellated margins, is the most common variety (Fig. 8a). Another type is represented by millimetre-scale nodules with mammillated surfaces. Both types contain plentiful gas/fluid-filled inclusions or empty micropores (Fig. 8b). The advanced recrystallization of the host dolomite does not allow us to interpret whether these presumed nodules formed by incorporative or displacive growth.

Lithofacies VII comprises laterally continuous, red or brown, fine-grained, thinly planar-laminated, micritic, allochemical dolarenites which are entirely developed in the uppermost part of Member H. Allochems are represented exclusively by dolomitic ooids. Dolostones contain relics of primary porosity (i.e. birdeyes) and vugs filled with cryptocrystalline quartz.


(a)
(c)
(e)
(d)
(b)
(f)

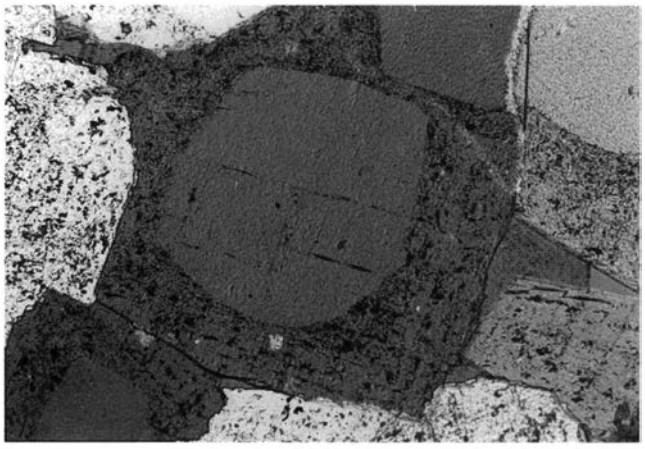

Fig. 6. Syntaxial dolomite spar overgrowth on a dolomite clast (recrystallized ooid?). Member B dolarenite. Cross-polarized light. Drillhole 4699, depth 506.0 m. Long axis of photomicrograph is 1.2 mm.

Lithofacies VIII is represented by dolostone breccias, which occur in the lower and upper parts of Member A, at the base of Member C, and in the upper part of Member D. In all cases, breccias are clast-supported and appear as poorly cemented angular fragments of brown, pink and white dolostones embedded in insoluble residue that commonly consists of dark brown dolomite–sericite–chlorite material rich in iron oxide. In some cases dolostone layers lying immediately above the breccia are largely intact, though they become gradually jointed and consequently produce clasts into the breccia.

Lithofacies IX is represented by magnesites and magnesite-rich dolostones forming 3–15 m-thick beds in Members A, B and D. Magnesites are white, grey, yellowish, fine- to coarse-grained, structureless rocks. The magnesite lithofacies has been discussed in detail by Melezhik et al. (submitted).

Lithofacies X is a stromatolitic mat lithofacies forming persistent beds of variable thickness, columnar stromatolites and a variety of biostromal and biohermal columnar stromatolites. In places stromatolites have well-pronounced pink and red colours (Fig. 9) and they have thus been termed 'red beds'. Columnar stromatolites and oncolites are very abundant in Members B, C, D and G. In places stromatolitic beds are deformed into tepee structures (Akhmedov et al. 1993). Breccias of stromatolitic dolostones related to the tepee structures have been observed in Member F (Fig. 5d). Flat-laminated stromatolitic layers of Members A and E have always been observed to be multicoloured, highly cracked and syngenetically brecciated (Fig. 5e).

Detailed description of the stromatolitic lithofacies is presented in the following section.

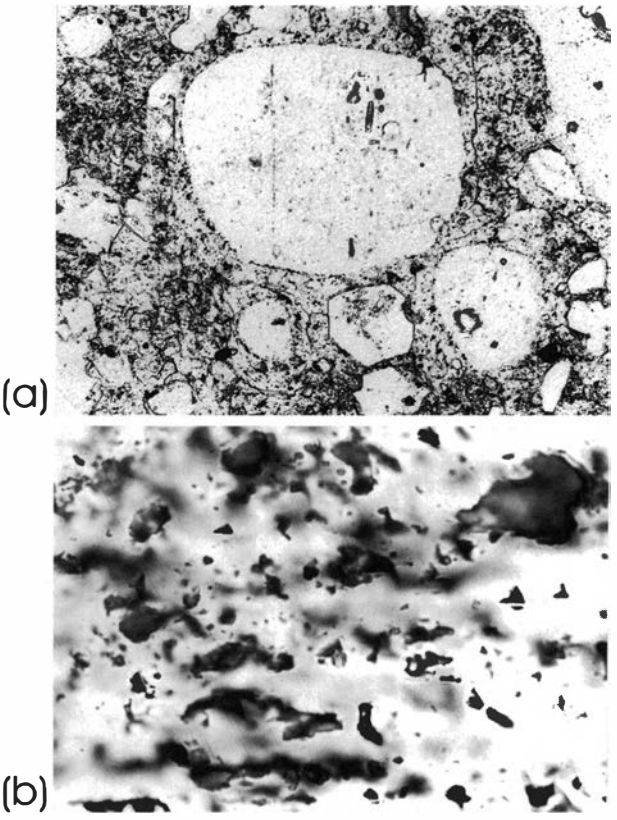

Fig. 7. (a) Photomicrograph of dolarenite from Member B. The dolarenite is composed of recrystallized ooids and dolostone clasts in a 'dusty', sparry dolomite matrix. Plane-polarized light. Drillhole 4699, depth 522.5 m. Long axis of photomicrograph is 1.2 mm. (b) Gas/fluid inclusions in dolomite spar, matrix of Member F dolarenite. Plane-polarized light. Drillhole 5177, depth 392.7 m. Long axis of photomicrograph is 0.1 mm.

Fig. 5. Photographs of drillcore illustrating sedimentological features of rocks of the Tulomozerskaya Formation ('b–e' are from Melezhik et al. 1999). (a) Dolomite-pseudomorphed crystals of sulphate. Drillhole 4699, depth 651.8 m. Member A siltstone, Lithofacies IV, low-energy, barred lagoon under evaporitic conditions. (b) Bedding surface between two pale pink dolostone layers extending from upper left to lower right corner. The bedding surface is marked by desiccation cracks filled with sandy material (pale grey). Drillhole 5177, depth 604.0 m. The lowermost part of Member D, Lithofacies V, upper tidal or peritidal evaporitic setting. (c) Red, structureless dolorudite. Intraclasts are dolomite ooids (white and grey) and red, hematite-rich, sparry and micritic dolostones (red). Drillhole 4699, depth 535.5 m. The lower part of Member B, Lithofacies VI, barred evaporitic lagoon. (d) Red breccia of stromatolitic dolostones related to a tepee structure. Note marginal reddening of some of the fragments (lower right corner), which suggests that the breccia was exposed to air and subjected to oxidation. Drillhole 5177, depth 670.0 m. Member C, Lithofacies X, upper tidal or supratidal zone of carbonate flat. (e) Red, flat-laminated, weakly domed stromatolites with fenestrae (blister stromatolite). Stromatolite laminae are cracked and syngenetically brecciated, which resulted in the development of a clotted fabric. Drillhole 5177, depth 660.0 m. Member C, Lithofacies X, drained depressions and ephemeral ponds in a supratidal carbonate flat. (f) Red, finely planar-laminated, and low-angle cross-stratified siltstone. Note light-coloured bleaching zones and 'roll structure' developed along more permeable sandstone layers. Bleaching is due to the introduction of reducing solutions to the red siltstone. Solutions were likely derived from overlying C_{org}-rich sediments of the Zaonezhskaya Formation during late diagenesis–catagenesis. The beds are transitional from the Tulomozerskaya to the Zaonezhskaya Formation, lacustrine environment. Core diameter in all cases is 42 mm.

Biofacies

In general, stromatolite-forming algae interact in a complex way with environmental conditions, both at microscopic and macroscopic levels (Cohen et al. 1977;

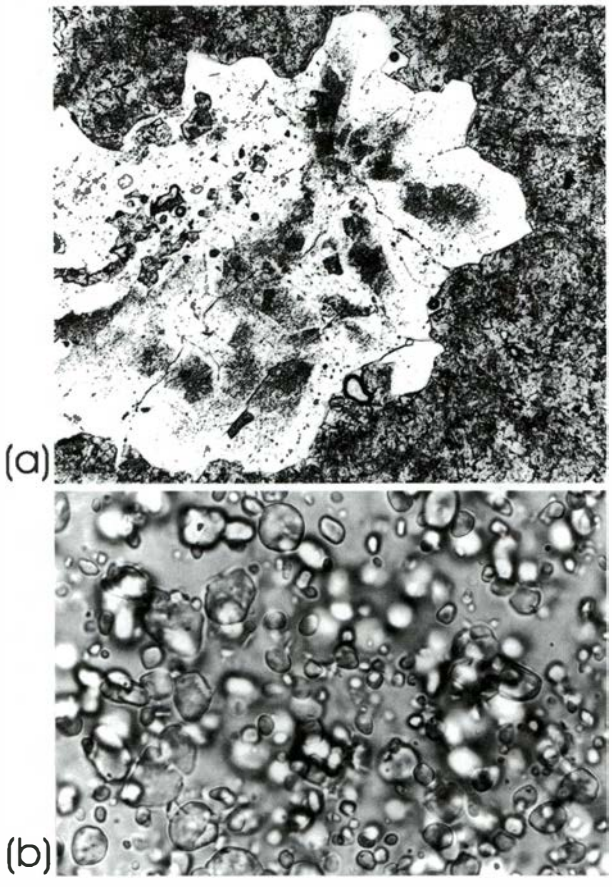

Fig. 8. (a) Photomicrograph of quartz aggregate with crude radiating structure. Member B sparry allochemical dolostone. Quartz with cloudy appearance due to the presence of gas/fluid inclusions. Plane-polarized light. Drillhole 4699, depth 524.1 m. Long axis of photomicrograph is 3.0 mm. (b) Gas/fluid inclusions in radiating aggregate of quartz. Member B sparry allochemical dolostone. Plane-polarized light. Drillhole 4699, depth 535.5 m. Long axis of photomicrograph is 0.1 mm.

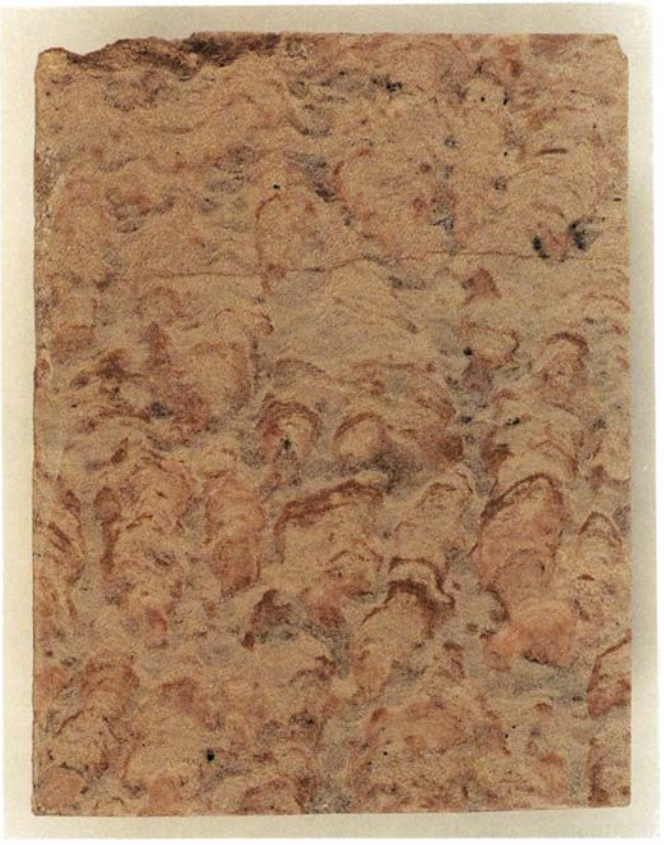

Fig. 9. Red, columnar stromatolites from Member C. Note intercolumnar space filled with light grey and white dolarenite, whereas the stromatolite laminae and the margins of column are composed of pink dolomite. The pink colour is interpreted to have formed due to photosynthetically-induced precipitation of iron oxide in an extremely shallow-water environment.

Krumbein et al. 1977). As no reliable microfossils have been detected in the drillcores, our biofacies is limited to macroscopic study of stromatolite morphologies. Strictly speaking, stromatolites are organosedimentary structures produced by sediment trapping, binding and/or the precipitation activity of micro-organisms, primarily cyanobacteria (e.g. Walter 1976; Monty 1976; Pentecost & Riding 1986; Burne & Moore 1987; Fairchild 1991).

Biostromal and biohermal columnar stromatolites of the TF come in a diverse array of sizes and shapes (Makarikhin & Kononova 1983). Figs. 3 and 4 summarize the distribution of the principal stromatolite morphologies vs. stratigraphy. Some of these stromatolite developments have been found in the drillholes studied, though most have been described from outcrops near the drilling site. The stromatolite morphologies may be grouped into the following types:

1. Flat-laminated, fenestral stromatolites forming low-relief sheets are characteristic features of Members A and E. They have also been documented in the lower part of Member B and in the middle parts of Members C and F. The laminated stromatolites developed on a carbonate substrate (Fig. 10a). Laminae shapes vary from wrinkled on the 1–2 mm scale, to weakly domed on the 3–5 mm scale (blister stromatolite mat). Red dolomite, composing wrinkled and weakly domed stromatolite laminae, is rich in hematite. The laminated stromatolites are very commonly cracked and appear as either an indistinct, clotted fabric (Fig. 5e, 10b) or a ribbon fabric with polygonal prism cracks. Common developments are inorganic laminations with algal

Fig. 10. Photographs of drillcore and outcrops illustrating sedimentological features of the Tulomozerskaya Formation stromatolites. (a) Structureless dolarenites (light brown, lower half of drillcore) serve as substrate for weakly domed stromatolites, which are, in turn, overlain by flat-laminated stromatolites. Member G, Lithofacies X, shallow water near shore zone. Drillhole 5177, depth 360.0 m. (b) Pink, weakly domed and flat-laminated stromatolites are cracked and separated by dolarenite with the development of an indistinct, clotted fabric. Member B, Lithofacies X, ephemeral ponds on supratidal zone. Drillhole 4699, depth 520.4 m. (c) Bedding surface of flat-laminated stromatolites with polygonal desiccation cracks. Note globular stromatolite with indistinct boundaries developed within individual polygons (lower left corner). Member B, Lithofacies X, supratidal zone. Southwestern shore of Sundozero Lake. (d) Bedding surface of biostrome (columnar *Nuclephyton confertum Mak.*) in sharp, subvertical contact with crudely bedded dolarenite. Note smaller columns developed along the biostrome margin. Member B, Lithofacies X, intertidal zone in a protected lagoon. Southwestern shore of Sundozero Lake. (e) Elongated columns of *Nuclephyton confertum Mak.*, bedding surface. Member B, Lithofacies X, intertidal setting. Southwestern shore of Sundozero Lake. Core diameter is 42 mm, length of knife 24 cm.

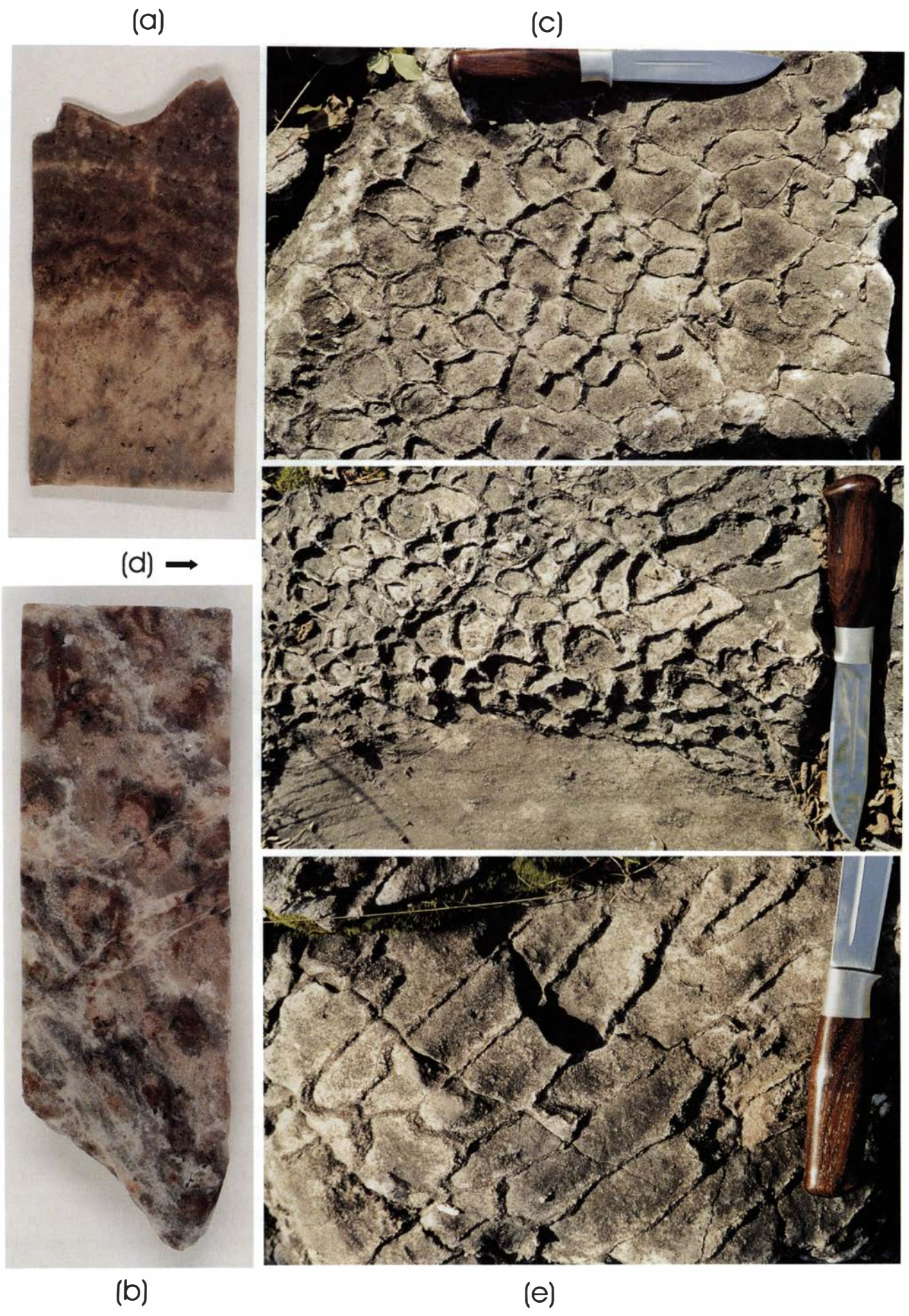
(a)
(c)
(d)
(b)
(e)

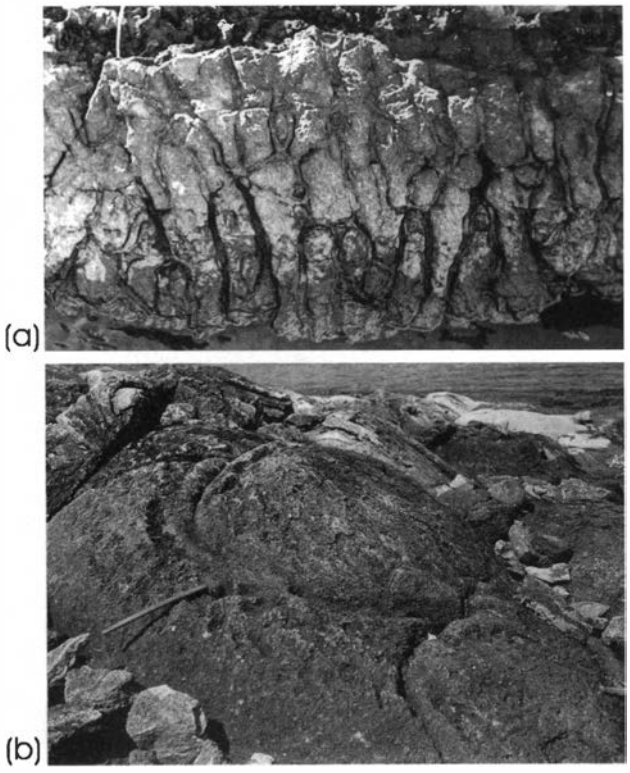

Fig. 11. Stromatolite morphologies. (a) *Parallelophyton raigubicum Mak.* Ridge structure on the surface of biostrome. Member B, Lithofacies X, intertidal zone exposed to wave action. Length of outcrop is 125 cm. (b) Cupola-like bioherm composed of *Carelozoon metzgerii Mak.* Southwestern shore of Sundozero Lake near Raiguba. Member B, Lithofacies X, shallow water near shore zone. Length of hammer is 70 cm. Both photographs are reproduced from Makarikhin & Kononova (1983).

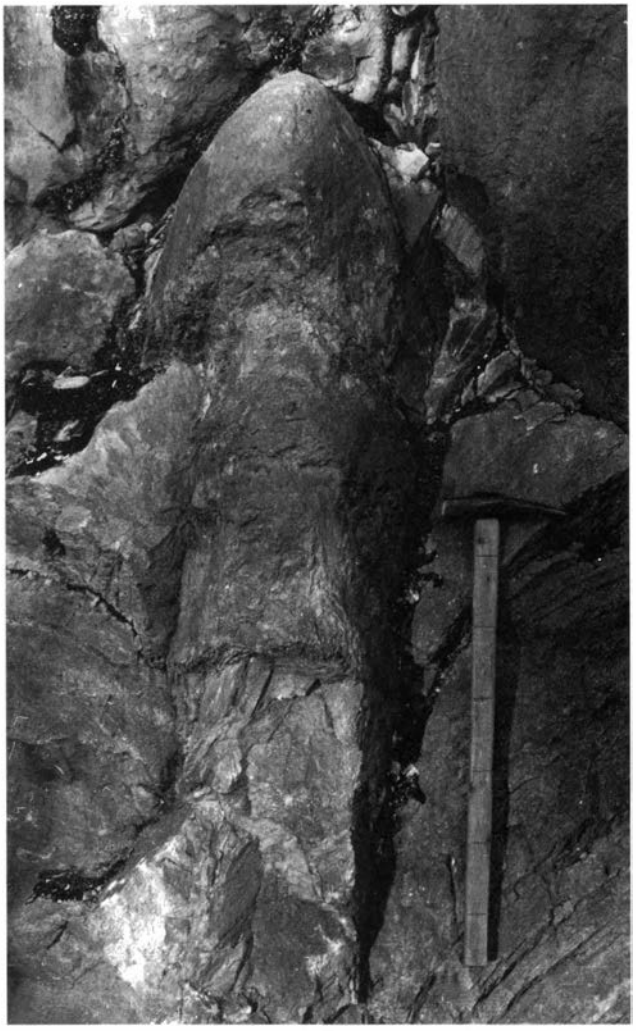

Fig. 12. Large column of *Colonnella carelica Mak.sp.nov.* Member D, Lithofacies X, subtidal zone. West face of Kintsiniemi quarry near Little Janisjarvi Lake. Length of hammer is 70 cm. Photograph is reproduced from Makarikhin & Kononova (1983).

partings. Desiccation cracks that developed on surfaces of the flat-laminated stromatolites apparently led to the nucleation and formation of globular stromatolites with indistinct boundaries, which occupy the space within individual polygons (Fig. 10c).

2. Laterally continuous biostromes are the most abundant type showing the development of columnar stromatolites. The stromatolites are characterized by smooth, simple convex laminations. The thickest (2–3 m) biostromes have been documented in the middle part of Member B where they are composed of markedly divergent columns of red *Sundosia mira (But).* Another type of markedly divergent columnar stromatolites, red *Carelozoon jatulicum Metz.*, composes thick (up to 2 m) biostromes in the middle part of Member C. Biostromes of *Nuclephyton confertum Mak.* (branching columnar stromatolites) are composed of tightly packed columns. The columns are larger in the middle parts of the bioherms, becoming smaller – fining towards the margins – and in sharp contact with surrounding intraclastic dolostones (Fig. 10d). Laminae of stromatolites consist of red, hematite-rich dolomite. A series of biostromes in the upper parts of Members B and C consists of tightly packed, elongated columns (Fig. 10e). They have gently arched upper surfaces with a ridged morphology (Fig. 11a). *Omachtenia kintsiensis Mak.* and branching columns of *Djulmekella sundica Mak.* form thin biostromes in Members C and H, respectively.
3. Very close-spaced bioherms with convex-up domes 0.8 m wide and very gently dipping margins are separated by either pale grey, laminated, fine-grained dolostones or red, hematite-rich, structureless dolorudites containing oncolites *Radiousus sp.* This type of bioherm is found in the uppermost part of Member G.
4. Spaced bioherms are most abundant in the middle of Member B (Fig. 4) where they are surrounded by red, hematite-rich, structureless dolostones. These bioherms are commonly composed of markedly divergent, branching columnar stromatolites and form cupola-like buildups 3–5 m wide and 1.5 m high with steeply dipping margins (Fig. 11b). The synoptic relief of the stromatolite domes above the surrounding sediment surface is difficult to determine. Based on sporadically observed single laminae enveloping the full height of

the bioherm, one may suggest that the synoptic relief was at least 20 cm.

5. Spaced, single, large columns of *Colonnella carelica Mak.* are 0.2 m wide and up to 1.5 m high. Columns are either tightly packed or largely separated by grey laminated dolostones (Fig. 12) and are composed of grey and pale grey, diffuse laminae consisting of dolomite rich in clastic quartz. This type of stromatolite morphology is rather rare and a typical feature of the lower part of the Member D.
6. Oncolites have been documented throughout the sequence, although they are most typical for Member G and for layers associated with magnesite (Figs. 3, 4).

Discussion

Palaeoenvironmental interpretation of terrigenous and non-stromatolite carbonate lithofacies

Lithofacies I. – Main diagnostic features of the Lithofacies I rocks are the dominance of sand material, lack of silty and muddy particles, unidirectional cross-stratification, generally fining-upward sequence, and presence of fining-upward erosional channels. These features are consistent with braided fluvial systems over a low-energy river-dominated coastal plain.

Lithofacies II. – The sedimentological information available is not sufficient to make a reliable palaeoenvironmental interpretation. The lenticular bedding suggests that the mixed sand- and mud-sized fractions were deposited from asymmetrical currents. This indicates that at least part of the Lithofacies II sediments might have formed in a tidal setting. An apparent lack of reworking is indicative of a low-energy environment. Overall the data may be consistent with an upper tidal zone protected from wave action.

Lithofacies III. – This lithofacies has many similarities with terrestrial 'red bed'–dolostone–halite association reported from the Bitter Spring Formation in the Amadeus Basin, Australia (Southgate 1986), which was reported to have formed in a series of shallow hypersaline lakes and ponds.

The presence of halite pseudomorphs and absence of calcium sulphate evaporites in the Lithofacies III is also consistent with a non-marine origin of red mudstone–siltstone–sandstone association. Considering abundant desiccation cracks and the presence of small-wavelength wave ripples, a playa lake environment may be proposed. The amygdaloidal structure of the basalt supports a subaerial environment.

Lithofacies IV. – The bi-directional cross-beds observed suggest that they apparently form by the reversal of current direction during a tidal cycle. The flaser bedding might have been produced by asymmetrical currents. Based on these observations and on the fact that erosional furrows and ridges related to wave action have not been observed, the Lithofacies IV sediments may be assigned to a low-energy, protected intertidal setting such as a barred lagoon or bight. Sulphate pseudomorphs indicate evaporitic conditions.

Lithofacies V. – Sporadically developed desiccation cracks filled with sandy material indicate that the dolostones were episodically exposed to air and the quartz, sandy material was introduced from land. The desiccation cracks do not bear signs of post-depositional compaction, thus suggesting that the lithification occurred prior to burial. Consequently, the depositional setting was episodically affected by long-term subaerial exposures, so the carbonate sediments had enough time to have been lithified prior to their burial.

The observed 'swallow tail' twin morphology of dolomite pseudomorphed small crystals of gypsum closely resembles those which have been reported from ancient rocks elsewhere (Rubin & Friedman 1977; Spencer & Lowenstein 1990). In recent environments gypsum commonly grows from groundwater brines within permeable sediments in the phreatic zone, the vadose zone, and at the subaerially exposed sediment surface of desiccated playas and sabkhas (Kendall 1984; Demicco & Hardie 1994). Displacive intrasediment growth of gypsum producing isolated euhedra (similar to those found in Lithofacies V) is commonly reported from within brine-logged marginal marine and marginal lacustrine sediment of modern evaporitic environments (Masson 1955; Kinsman 1966). Intrasediment gypsum growth provides unequivocal evidence of post-depositional crystallization in an evaporitic environment (Demicco & Hardie 1994). However, interpretation is not straightforward when ancient gypsum is concerned. It is generally difficult to distinguish between gypsum precipitated penecontemporaneously from shallow, near-surface brines and later diagenetic growth from deep formation brines during burial (Hardie et al. 1985; Spencer & Lowenstein 1990).

Similar obstacles apply for the interpretation of the Lithofacies V gypsum pseudomorphs. No time constraint for the gypsum growth is available. However, if the gypsum was growing diagenetically from deep formation brines during burial, this would imply the formation of the same type of gypsum throughout the whole sequence of underlying sediments. As this has not been observed the penecontemporaneous precipitation from shallow, near-surface brines seems to be more plausible.

The association of desiccation joints and abundant evaporite minerals is evidence of emergence and definitely indicates that the micritic dolostones of Lithofacies V seem likely to be of a shallow-water, evaporative origin. A similar genesis has been suggested by Fairchild & Hambrey (1984) for abundant fine-grained, sulphite-bearing dolostones of D4–D6 members in the Vendian Dracoisen Formation, northeastern Spitsbergen.

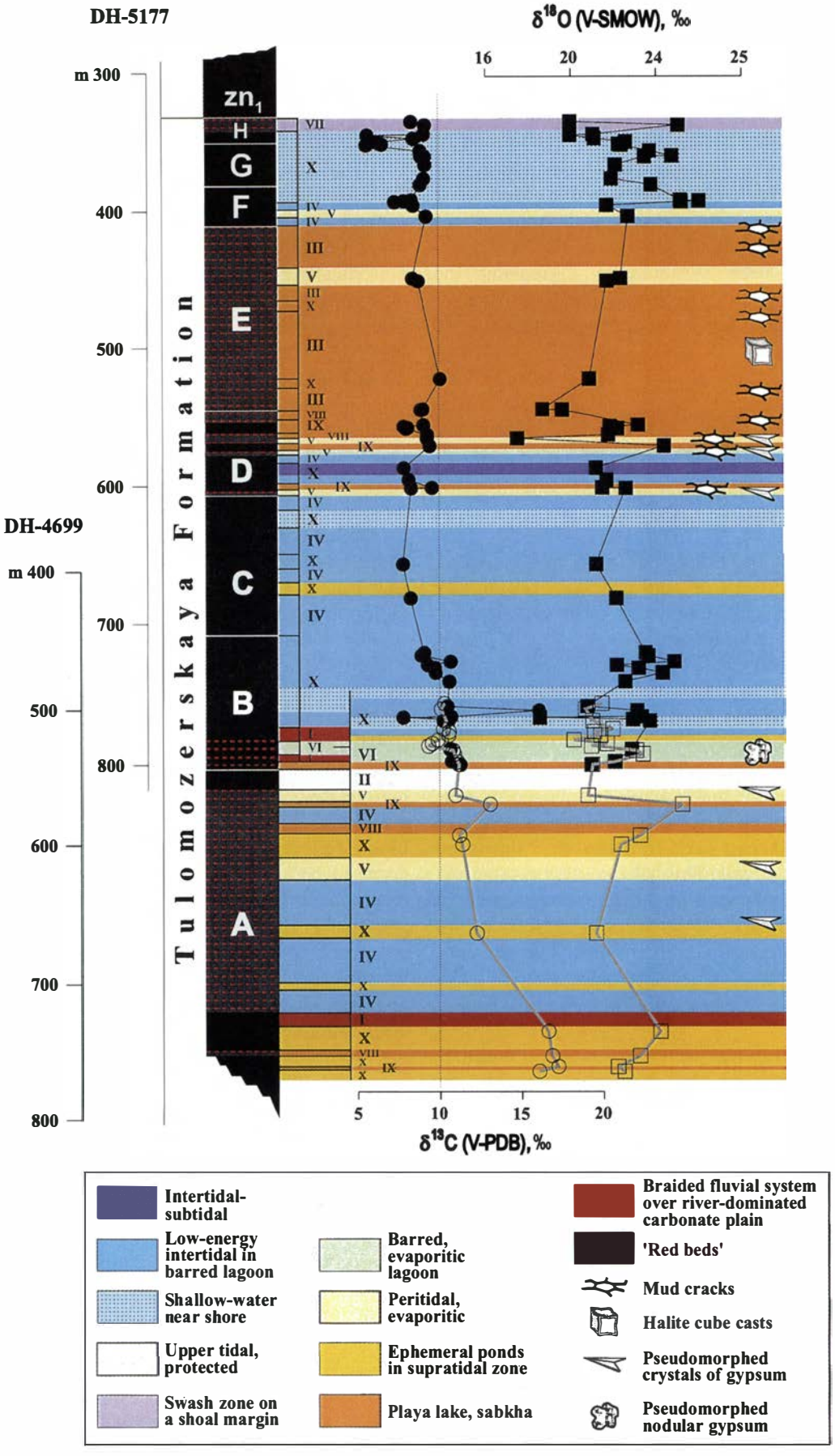

Fig. 13. Carbon and oxygen isotope values vs. lithostratigraphy and inferred palaeoenvironmental settings. Analytical database is from Melezhik et al. (1999).

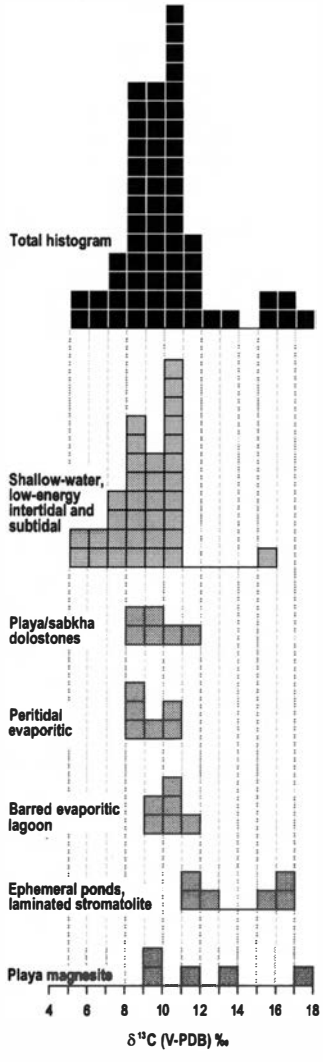

Fig. 14. Histograms of $\delta^{13}C$ values of dolostones and magnesites formed in different environments. Analytical database from Melezhik et al. 1999 (all diagenetically altered samples with Mn/Sr >10 are excluded).

The significance of the tepee structures in Lithofacies VI can be demonstrated by both recent and ancient examples. In general, tepee structures can develop in both a submarine environment and at, or near, a subaerially exposed surface. The modern environment of an arid or semi-arid climate along a coastal plain is considered to be most favourable for the development of massive tepees, as evidenced by modern Australian coastal plain environments, where tepees are reported from surface crust (e.g. Handford et al. 1984). There are at least two important settings for the development of extensive tepee zones in ancient carbonate deposits. One has been described from the Precambrian Rocknest Formation (Wopmay Orogen, Northwest Territories, Canada, Grotzinger 1986) and Permian Carlsbad Group (Guadalupe Mountains of West Texas and New Mexico, Adams & Frenzel 1950). These are associated with a shallow peritidal or island environment (an exposed barrier) located at the seaward margin of carbonate platforms (e.g. Demicco & Hardie 1994). Other, Triassic examples signify subaerial exposure of the carbonate platform for extended periods due to lower amplitude sea-level low stands (Hardie et al. 1986; Goldhammer at al. 1990).

Thus, apparently both options, namely a shallow peritidal environment located at the seaward margin of a carbonate platform, and a carbonate platform subaerially exposed for extended periods due to lower amplitude sea-level low stands, may be equally applicable for Lithofacies V.

Considering all the sedimentological features, a peritidal, evaporitic environment on the carbonate platform, which was frequently emerged for extended periods, seems appropriate.

Lithofacies VI. – Coated grain lithofacies are generally known to accrete in shoal environments where currents are sufficiently strong to move grains periodically along the sea floor (Bathurst 1976). Given that the lack of micrite is a primary feature of the Lithofacies VI dolarenites and dolorudites, the depositional setting requires current or wave energy to be strong enough to winnow away the fine matrix (Folk 1962). However, the unsorted, both rounded and angular character of intraclasts suggests that the depositional environment has only occasionally been influenced by such currents and waves.

Another diagnostic feature of Lithofacies VI is its abundant cauliflower-like aggregates of quartz. The shapes of individual crystals of quartz resemble those of gypsum, whereas the aggregates are similar in shape to anhydrite or gypsum nodules reported from the Late Proterozoic sequence of northern Norway (Siedlecka 1976; Tucker 1976), Vendian succession of northeastern Spitsbergen (Fairchild & Hambrey 1984) and the late Vendian Canyon and Spiral Creek formations in East Greenland (Fairchild & Herrington 1989).

Discovery of solitary anhydrite nodules, tens of millimeters to 0.25 m in diameter, in the Holocene sediments of the Persian Gulf (Curtis et al. 1963; Shearman 1966) led to the development of 'carbonate–evaporite' or 'sabkha' depositional models to explain some ancient shallow-marine carbonate deposits (Shinn 1983; James 1984; Hardie & Shinn 1986). However, there are several problems with interpreting the significance of anhydrite nodules and presumed pseudomorphs (for details, see Demicco & Hardie 1994, pp. 201–206) like those found in Lithofacies VI. Although nodular gypsum and anhydrite are characteristic of deposition of evaporites under subaerial sabkha environments, they are not unequivocal criteria of such a condition (Demicco & Hardie 1994). This has been acknowledged by Fairchild & Herrington (1989) who interpreted the calcite–quartz pseudomorphs after calcium sulphate nodules of the late Vendian Canyon and Spiral Creek formations in East Greenland to have formed in subtidal sediments by incorporative growth from intraformational brine. However, the model suggested by Fairchild & Herrington (1989) also seems disputable; at least some nodules exhibit clear displacive growth (Fair-

child & Herrington 1989, Fig. 14b), which is unlikely to be consistent with the proposed mechanism.

In summary, overall sedimentological features of Lithofacies VI, though of acknowledged limitation, point to a shallow-water, relatively low-energy evaporative environment. Lithofacies VI could be a barred lagoon or bight occasionally influenced by tidal currents and waves.

Lithofacies VII. – This lithofacies is only developed in Member H. The laterally continuous, sheet-like beds of planar-laminated ooidial dolostones most likely formed in the swash zone on the margin of a shoal complex. The absence of stromatolites apparently indicates highly mobile substrates. The red colour is consistent with the frequent exposure of Lithofacies VII to the oxygenated air.

Lithofacies VIII. – The clast-supported dolostone breccias are not related to palaeokarst surfaces. Instead, field observations suggest that the breccias have been generated by the interstratal solution episodes. Although a robust palaeoenvironmental interpretation of Lithofacies VII is hampered by limited field observations on the lateral extension of the layers containing breccias, the sedimentological features available are consistent with solution collapse breccias. In general, solution collapse breccias are considered to be important features of carbonate–evaporite successions (Demicco & Hardie 1994). In the studied case the breccias are associated with either the upper part of a shallowing-upward dolostone sequence (intertidal–peritidal–ephemeral ponds, Member A, Fig. 13) or the sabkha–playa magnesite (Member D, Melezhik et al. submitted). These associations, together with the sedimentological features observed, suggest that the dissolution collapse breccias may be assigned to a playa lake or sabkha setting.

Lithofacies IX. – The magnesite lithofacies has been discussed in detail by Melezhik et al. (submitted). They have reported that the Tulomozerskaya magnesite formed in sabkha (similar to sabkha magnesites of Abu Dhabi, Bush 1973) and playa environments (similar to the Coorong Lagoon district and Lake Walyungup coastal playa magnesites, Australia, Walter et al. 1973; Schroll 1989; Coshell et al. 1998).

Palaeoenvironmental interpretation of stromatolite morphologies ('biofacies')

It has been shown (for references see Golubic 1976) that the specifically different environmental requirements of cyanobacteria have resulted in their distribution and dominance being dependent on environmental conditions and constraints. Within these constraints, environmental factors may additionally affect stromatolite morphology. In principle, stromatolite morphologies may be an interplay of several factors, such as light, wetness, salinity, bottom traction, sedimentation rate, abrasion by particles, and rate of induration (Logan 1961; Gebelin 1969; Bathurst 1976). Numerous detailed studies of Precambrian stromatolites vs. palaeoenvironments have been published in the last few decades. However, there are only very few examples of calcified stromatolites from recent times, which provide a direct link between different stromatolite morphologies and environmental settings. Among them are stromatolites known from the Bahamas-Florida platform, Persian Gulf and Shark Bay, Western Australia.

The first paper on the Hermelin Pool (Shark Bay) stromatolites claimed that they were restricted to the intertidal zone, and this concept was erroneously extended to the interpretation of ancient stromatolites (Logan 1961). Subsequent investigation showed the existence of widespread subtidal stromatolites (Playford & Cockbain 1976). Later, Burne & James (1986) suggested that the present-day intertidal columnar forms originated as subtidal stromatolites, which were later stranded as a result of a relative fall in sea level. However, Playford (1990) claimed that there are many stromatolite forms which have grown wholly in the intertidal zone. Golubic (1985) reported a series of discrete mat communities which occupies well-marked out zones in Shark Bay within permanently submerged to supratidal environments. Hoffman (1976) and Playford & Cockbain (1976) have demonstrated that discrete columnar forms (0.4 m high) occur on headlands fully exposed to waves, and have been found in subtidal and intertidal environments. The relief of the columns is proportional to the intensity of wave action. Elongated columns, with elongation developed parallel to the direction of wave attack, form in less exposed bights near headlands. Ridge and rill structures with reliefs of 0.1–0.3 m occur in areas partially protected from wave attack. Small embayments completely protected from waves are represented by stratiform sheets with lower relief.

Surprisingly, some non-marine stromatolites exhibit a similar dependence from bathymetry. The Lake Tanganyika stromatolites are one example of these. The original depth range for stromatolite growth morphologies includes (Cohen et al. 1997): small column and encrustation (1.5–14 m) – large isolated domes and columns (5–15 m) – large linked domes and columns (19–19 m) – bioherms (19–27.5 m).

Numerous detailed studies of Precambrian carbonate facies also suggest a relationship between bathymetry and stromatolite morphologies. Fairchild & Herrington (1989) described a clear connection between bathymetry and the distribution of microbial structures in the late Vendian sequence from east Greenland. Thin dolomitic stromatolites formed in the upper part of the shoreface. Abundant biohermal stromatolites with moderate to zero synoptic relief occurred in the lagoonal setting. Where exposure was more frequent, synoptic relief is <10 cm. No stromatolite has been recorded in an inferred supratidal zone. However, study of Upper Riphean (Svalbard) microfossil assemblages has shown that stratiform stromatolitic mat accreted in supratidal and upper intertidal environments (Fairchild et al. 1991). Another example of the late Precambrian biostromal, non-columnar, head- and

washbowl-shaped stromatolites accreted in supralittoral freshwater ponds has been reported from Varanger Peninsula, Norway (Siedlecka 1982).

Palaeoenvironmental distribution of microfossils and stromatolites from the Upper Proterozoic Blacklundtoppen Formation in Spitsbergen (Knoll et al. 1989) demonstrated a clear link between depositional settings and various forms of stromatolites. Low domical stromatolites, 20 cm high and 30 cm wide, formed within an 'inhospitable' set of peritidal environments. Columnar stromatolitic bioherms, 1.5 m high, accreted in peritidal environments, which were characterized by episodic wave and current activity. Spaced conical stromatolites accumulated subtidally below a storm wave base.

In other regions upper Proterozoic laterally persistent coniform biostromes have been assigned to quiet subtidal conditions (Bertrand-Sarafati & Moussine-Pouchkine 1985, 1988; Kerans & Donaldson 1989).

Grotzinger (1989), describing stromatolitic reefs and buildups on Precambrian carbonate platforms, reported a clear link between facies distribution and stromatolite morphologies. Laminated stromatolites are attached to tide flats; stromatolite mounds and branching columns with very strong elongation are characteristic of intertidal zones in forereefs and shallow ramps affected by wave action, whereas conical stromatolite bioherms are accreted subtidally.

Using the criteria outlined above as well as both modern and ancient examples of different stromatolite morphologies as indicators of depositional settings, the studied stromatolites have been interpreted in terms of basinal environments. A brief summary of these reconstructions is presented below.

Lower relief, flat-laminated, fenestral stromatolite sheets. – This type of stromatolite in the TF resembles many stratiform stromatolitic mats reported from various Precambrian carbonate formations. It is somewhat similar to the Upper Riphean stratiform stromatolitic mats from Svalbard, which accreted in supratidal and upper intertidal environments (Fairchild et al. 1991). Intertidal stratiform stromatolites from the Upper Proterozoic Bitter Spring Formation are also examples (Southgate 1986). Proterozoic laminated tufa and microbial laminates accumulated on an intertidal to supratidal, low-energy tidal flat (Kah & Knoll 1996) comprise another representative of this type of stromatolite morphology.

Based on the examples and criteria outlined above, it can be posited that the lower relief, flat-laminated stromatolite sheets of the TF might have formed in an environment where wave and tidal scour was weak. This may have developed throughout an intertidal zone of protected embayments, as well as in protected embayments and protected parts of an upper intertidal zone in bights (see Shark Bay stromatolites, Hoffman 1976). The presence of blister, clotted fabrics with fenestrae requires a lower supratidal zone (e.g. Hoffman 1976). However, the variegated colour, highly cracked and syngenetically brecciated character of the flat-laminated stromatolite sheets may suggest that they formed in drained depressions and ephemeral ponds in a supratidal or upper tidal zone of a carbonate flat. This type of environment is assigned entirely to Member A (Fig. 3) and to the lowermost dolostones of Members B and C.

Laminated, fenestral stromatolites of the upper part of Member F are marked by variegated colour and tepee-related brecciation. These sedimentological features are similar to those described from Precambrian (e.g. Fairchild et al. 1991) and modern (e.g. Ferguson et al. 1982) examples of fenestral carbonate lithofacies found in broadly supratidal settings.

The flat-laminated stromatolite lithofacies of Member E are interbedded with Lithofacies III red siltstones containing halite casts. This closely resembles the dolostone–halite–terrestrial 'red beds' association of the Bitter Spring Formation, which formed in shallow hypersaline lakes and ponds (Southgate 1986). Similarly, the flat-laminated stromatolite lithofacies of Member E is assigned to a playa lake environment.

Laterally continuous biostromes. – The biostromes, mostly composed of small branching columnar stromatolites, are the next most abundant type of stromatolite lithofacies. In general, this stromatolite morphology may form in intertidal (Hoffman 1976) and subtidal (Southgate 1986) environments. As the intertidal substrate is unstable, stromatolitic mats cannot colonize loose sand, and can initially only be established on lithified crusts in order to develop further discrete columns. The small diameter and low relief of branching columns in the TF place further constraints on the depositional environment. Such stromatolite morphologies are consistent with intertidal settings in protected bights, as is again evident from the Shark Bay example (Hoffman 1976). This assignment is also supported by the development of small-scale ridged structures, which are typical features of Members B and C *Parallelophyton.*

Spaced bioherms, very close-spaced bioherms, spaced, large, and, in places, solitary columns. – These stromatolite morphologies are rare in the TF. They have been found in the middle parts of Members B, C and the lowermost portion of Member C. Spaced columns and spaced bioherms, particularly those of Member G, are associated with abundant oncolites (Fig. 4). The spaced bioherms of the TF show many similarities to the late Proterozoic Draken bioherms from Spitsbergen (Swett & Knoll 1985). Tentatively, the Tulomozerskaya spaced bioherms may be assigned to a similar, shallow-water, near-shore marine environment.

In general, discrete columnar stromatolitic structures occur in such modern environments where wave and tidal scour are strong. Consequently, their relief is proportional to wave action (Hoffman 1976). Similarly, we suggest that these particular stromatolites of the TF may indicate intertidal settings close to shorelines fully exposed to wave

action. Alternatively, they might have formed in subtidal settings. For example, in modern environments, large (up to 2 m high), solitary stromatolites are known from actively migrating areas of Bahamian ooid shoals (e.g. Dill et al. 1986). Abundant oncolites favour both assumptions (e.g. Tucker & Wright 1990, p. 10).

Palaeoenvironmental significance of the 'red beds'

Considerable differences in colour between subtidal and high intertidal sediments have been documented in some modern carbonate environments (Shinn 1983). Even more striking contrasts in colour may be found between aqueous and terrestrial sediments (e.g. Southgate 1986). These are largely connected to the oxidation state of iron and the oxidation of organic matter.

Red coloration is an essential feature of the rocks of the TF, particularly of those developed in Members A, B, C, E, G and H. These rocks, together with the Lower Jatulian sequence, have been described in the literature as classic examples of Palaeoproterozoic 'red beds' (e.g. Sochava 1979). The designation 'red beds', which also includes stratiform and some columnar stromatolites, may be consistent with the presence of environments that were frequently exposed to air. Highly abundant and diverse stromatolites indicate that the Tulomozersky palaeobasin was characterized by very intensive microbial activity, which should have resulted in high bioproductivity. The red coloration and the lack of organic material seems to be the result of syndepositional transformation of the rocks, e.g., oxidation in sub-aerial conditions. In fact, there are several lines of evidence that the red colour is a primary phenomenon, caused by the presence of particles of hematite. In many cases, hematite enriches the steeper slopes of ripple marks as well as the bottom sets of cross-stratified beds (Sokolov et al. 1970). Breccia fragments in some of the tepee structures also show reddening, indicating that tepees were exposed to oxygen-containing air (Fig. 5d). Both micritic and sparry dolomite commonly contain fine particles of hematite. Many of the stromatolites display red coloration, which can be interpreted as a result of iron oxidation through photosynthetic activity of cyanobacterial mats (Fig. 9). Additionally, rocks subjected to postdepositional (catagenetic) alteration are represented by bleaching and discoloration of the 'red beds'. Bleaching occurs due to removal of oxidized iron by reducing solutions migrating within permeable layers. This resulted in the development of 'roll structures' (Fig. 5f).

The red colour developed throughout the TF suggests that the depositional settings, in which the 'red beds' were accumulated, might have been frequently emerged and exposed to air, thus being decoupled from the bordering marine environment.

Palaeoenvironmental significance of the dolostones

The overall bulk chemical composition of TF carbonate rocks approximates to a sandy dolostone with rare magnesite. Limestones have not been observed among the collected samples (Melezhik et al. 1999). Based on the Sr concentration and Sr/Ca_{dol} ratios, the dolostones of Member F and those of the upper part of Member G are consistent with a considerable alteration by meteoric water (Melezhik et al. 1999). The alteration of the dolostones of Member F has been assigned to a mixing zone where the meteoric component was high in Ca but lower in Sr. In contrast, the geochemical features of Members C, D, E and H dolostones have been ascribed to precipitation from a fluid resembling seawater. The latter group of dolostones implies that dolomitization was an early diagenetic phenomenon. This is consistent with observations obtained from other Proterozoic dolostones. Although processes and diagenetic environments involved in the formation of Proterozoic dolostones are different, many dolostones are similar in that they formed from early diagenetic fluids prior to deep burial (Tucker 1982, 1983b; Grotzinger & Read 1983; Zempolich et al. 1988; Kerans & Donaldson 1989; Fairchild et al. 1991).

A very clear distribution pattern has been reported for Neoproterozoic carbonate rocks. In general, Upper Proterozoic dolostones appear to correlate with evaporite, inter- to supratidal, and playa lake environments, or to be associated with C_{org}-rich stromatolites (Preiss 1987; Lindsay 1987; Southgate 1989; Knoll & Swett 1990). In contrast, limestones were deposited in basinal environments below a storm wave base (Adams & Cowie 1953; Germs 1983; Tucker 1983a).

Similarly, Delaney (1981) reported that a statistical pattern of basinal limestones and peritidal dolostones is common in Middle Proterozoic successions. The latter is exemplified by the thick carbonate formations of the McArthur Basin, northern Australia, where peritidal evaporitic, and playa lake carbonate rocks are dolostones, whereas shelf and basinal carbonate formations of the same age are composed predominantly of limestones (Muir et al. 1980).

Although in Palaeoproteozoic formations, stromatolitic or tufa-like dolostones (Grotzinger 1989) prevail over limestones, a distribution pattern similar to that observed in the Neoproterozoic has been recognized when carbonate depositional environments have been considered. All Palaeoproteozoic basinal carbonate rocks include substantial amounts of limestones (Ricketts & Donaldson 1981; Plumb et al. 1981; Beukes 1983; Hoffman 1989). In the Fennoscandian Shield, Palaeoproterozoic dolostones are closely associated with shallow-water, lacustrine environments within intracontinental rifts, whereas limestones appear to be correlated with the first development of large seas (Melezhik et al. 1997).

Overall, it does appear that Palaeoproterozoic to Neoproterozoic dolostones mark either peritidal evapori-

tic, and playa lake environments, which occur in areas of increased emergence and salinity, or lacustrine settings. Thus, the TF dolostones do not appear to be an exception.

Carbon isotopic records in the Tulomozerskaya succession

Although carbon isotope values for the TF dolostones have been reported in several papers (e.g. Yudovich et al. 1991; Karhu 1993; Akhmedov et al. 1993), the most extensive information involving the isotopic measurements of carbonate rocks throughout the entire sequence by using drillcore material has been given by Melezhik et al. (1999). The summary of this work is presented in Fig. 13, which demonstrates a vertical variation of $\delta^{13}C$ values through the Tulomozerskaya sequence based on 73 whole-rock analyses.

The overall spread of $\delta^{13}C$ values is from +5.6 to +17.2‰ (mean + 9.9 ± 2.3‰ vs. V-PDB, Melezhik et al. 1999). The carbon isotope values demonstrate an erratic decrease upwards in the sequence from +17.2‰ in the lowermost part of the Member A to +8.0‰ in Member C. Higher up in the succession, the $\delta^{13}C$ values are less variable and fall within the range +7.3 to +10.1‰. The only exception to this pattern is the four samples from the lower portion of Member H dolostones, with $\delta^{13}C$ of +5.6 to +6.6‰. Dolostones highly enriched in ^{13}C are located in the lowermost part of the succession (Member A), with one sample derived from Member B.

Environments with high $\delta^{13}C$ carbonate rocks and minerals: general

Isotopically heavy carbonates (higher than +2‰) are precipitated when a depositional system becomes depleted in the light carbon isotope, ^{12}C. Removal of ^{12}C may be achieved by several processes which can be of either local or global significance. Consequently, the amounts of isotopically heavy sedimentary carbonate rocks and minerals formed may range on a scale from very limited basinal to fairly large, regional or even global. Depositional environments that may lead to the formation of isotopically heavy sedimentary carbonates are as follows: (1) fermentative diagenetic systems, (2) hot springs, (3) saline evaporitic basins, (4) restricted, stromatolite-dominated basins, (5) closed basins with high bioproduction, and (6) stratified oceans. Some of the environments listed above have been discussed in detail in Melezhik et al. (1999). Further, we focus on those which can be applicable to the Tulomozerskaya dolostones.

Evaporitic basins precipitate ^{13}C-rich carbonate minerals by physical processes, namely evaporation effects and CO_2 degassing. Stiller et al. (1985) reported extreme ^{13}C enrichments (up to +16.5‰) in the dissolved inorganic carbon pool in evaporitic brines of the Dead Sea. However, Katz et al. (1977), studying deposits from the highly evaporated and saline Lake Lisian, found aragonite with $\delta^{13}C$ ranging from −7.7 to +3.5‰. Calcium and magnesium carbonate sediments formed in highly evaporative coastal sabkhas of Abu Dhabi, the Arabian side of the Persian Gulf (McKenzie 1981), have average $\delta^{13}C$ values of +3‰. Thus, even in highly evaporated systems, carbonate minerals with both negative and positive $\delta^{13}C$ values may be found (Bonatti et al. 1971; Pierre 1982; Magaritz et al. 1983).

However, Valero-Garsés et al. (1999) have reported extreme ^{13}C enrichment up to +13‰ in primary calcite and aragonite precipitates in saline, well oxygenated waters from high-altitude lakes in northwestern Argentina. The syndepositional enrichment in ^{13}C was solely attributed to physical processes, evaporation effects and CO_2 degassing.

A review of ancient evaporitic carbonate rocks formed at times of known high seawater $\delta^{13}C$ values shows that some Neoproterozoic carbonate rocks from NE Spitsbergen (Wilsonbreen Formation, Member 2) were characterized by enhanced $\delta^{13}C$ values, which were caused by evaporation in closed, glaciolacustrine environments (Fairchild 1991). Another Late Precambrian, Vendian example is provided by the D_5 dolostones of the Dracoisen Formation from the same region (Fairchild & Spiro 1987). Here, the dolostones exhibit extreme ^{13}C enrichment up to +11‰. This enrichment was assigned to a biologically-related mechanism or a 'Rayleigh distillation' kinetic effect during evaporation.

Late Permian dolostones and limestones exhibit both very pronounced enrichment in ^{13}C and clear evaporitic affinities. Beauchamp et al. (1987) suggested that the primary ^{13}C enrichment of the Permian Sverdrup Basin carbonate rocks (up to +7‰) as compared to the coeval ocean (+1 to +3‰) may only be explained if both global and local factors are involved. The latter was an intensive evaporation and ^{13}C enrichment of surficial brines through escape of CO_2 to the atmosphere during episodic closure of the basin. This factor was considered to have caused the formation of ^{13}C-rich carbonate rocks with highly elevated $\delta^{13}C$ values. Beauchamp et al. (1987) stated that the Permian isotopic evolution should be re-evaluated in terms of a global areal heterogeneity caused by local factors.

Restricted, stromatolite-dominated basins

On a basinal scale, enrichment in ^{13}C may be caused by widespread stromatolite-forming bacteria in shallow-water, closed or semi-closed environments (Des Marais et al. 1992a). As purely organic microbial mats are often characterized by very high organic productivity (Castenholz et al. 1992; Jørgensen et al. 1992), the rate of biological uptake of ^{12}C is higher than the rate of carbon diffusion to mat (Des Marais et al. 1992a). Consequently the dissolved inorganic carbon reservoir becomes rich in ^{13}C, resulting in both high $\delta^{13}C_{org}$ (−19.1 to +3.0‰) and high $\delta^{13}C_{carb}$ (+2.5 to +6.6‰) of recent stromatolitic mats (e.g. Des Marais et al. 1992a).

The above statement is also valid for carbonate-precipitating cyanobacterial mats (close analogues of stromatolite-building benthic Proterozoic communities) studied from many Australian lakes. In coastal lakes carbonate minerals precipitating on calcifying microbial mats have $\delta^{13}C$ values of +5 to +10‰ (Burne & Moore 1987). The high ^{13}C enrichment has been attributed to carbonate precipitation, which was biologically influenced by photosynthesis.

Surprisingly, in places, stromatolite-forming cyanobacteria from open marine environments may also induce the precipitation of carbonate minerals rich in ^{13}C. This situation has been reported in coralgal communities in Holocene high-energy reefs in Polynesia where associated thick stromatolitic micritic crusts, club-shaped and digitate micritic masses exhibit $\delta^{13}C$ values of +3.7 to +4.3‰. These values are highly elevated as compared to those measured from the modern (−3.2 to +0.4‰) and fossil (−2.0 to +1.9‰) *Acropora* from the same reef (Montaggioni & Camoin 1993). Although no explanation has been given by the authors, it is plausible that the ^{13}C enrichment was influenced by biological photosynthesis.

In contrast, special studies on Neoproterozoic marine stromatolites formed at times of known high seawater $\delta^{13}C$ did not reveal ^{13}C enrichment of carbonate minerals which were deposited by either biologically-induced precipitation or by mechanical trapping in cyanobacterial mats (e.g. Fairchild et al. 1990; Fairchild 1991). However, despite this general rule, some Neoproterozoic calcitic stromatolites formed in lacustrine environments are rich in ^{13}C compared to background limestones. This has been attributed to the precipitation related to enhanced photosynthesis in the neighbourhood of microbial mats (Fairchild 1991). A similar mechanism could have been suggested for the Vendian high $\delta^{13}C$ dolostones of the Dracoisen Formation (Member D_5) from NE Spitsbergen (Fairchild & Spiro 1987), discussed above.

Possible causes for high ^{13}C enrichment of the Tulomozerskaya dolostones

It has been discussed earlier (Melezhik et al. 1999) that none of the environments and processes outlined above, if they apply individually, could result in the $\delta^{13}C$ range observed in the Tulomozerskaya dolostones.

As far as the local factors are concerned, there are no indications of fermentative diagenesis, nor was a hot-spring environment involved in the formation of ^{13}C-rich dolostones (Melezhik et al. 1999). The general lack of organic material in the sequence leaves no credibility for the model which involves a closed lake with enhanced bioproduction. One may speculate that C_{org}-rich shungite rocks, which overlie the TF, are the distal facies to the ^{13}C-rich dolostones. This reconstruction of lateral facies relationships from a vertical sequence applies Walther's 'Law of Facies'. However, this exercise is not appropriate, as the C_{org}-rich shungite rocks – ^{13}C-rich Tulomozerskaya dolostone boundary coincides with the major erosional surface. Finally, the sedimentological features of the Tulomozerskaya carbonate rocks clearly suggest that both evaporative processes and biological photosynthesis in a semi-restricted or restricted, stromatolite-dominated basin can be applicable.

On other hand, it has been argued that enhanced accumulation of organic material worldwide is the most plausible model to explain the accumulation of Palaeoproterozoic ^{13}C-rich carbonate rocks (Baker & Fallick 1989a, b; Karhu 1993). But it is also true that existing global geological records contain no indication that accelerated accumulation of organic material took place prior to or synchronous with the deposition of ^{13}C-rich carbonate rocks (Melezhik & Fallick 1996). Consequently, a working hypothesis has been proposed that the highly elevated $\delta^{13}C$ values in Palaeoproterozoic carbonate rocks might have been driven by a series of factors, both global and local in nature (Melezhik et al. 1999). It has also been tentatively suggested that the global factors (i.e. accelerated accumulation of organic material) could have resulted in an isotopic shift of approximately 5‰. Thus, $\delta^{13}C$ values exceeding this isotopic shift could have been caused by a series of local factors which were superimposed on the global ones. At this stage we leave discussion of the global factors aside (for details, see Melezhik et al. 1999). As follows from the discussion presented above, among the local factors there are two which might be relevant, namely evaporative processes and biological photosynthesis in a semi-restricted or restricted, stromatolite-dominated basin. As outlined above, both of these factors are capable of enriching environments in ^{13}C, given a certain degree of basinal restriction. This is particularly true if the depositional environment was affected by syndepositional oxidation and consequent removal of C_{org}, as can be observed in the Tulomozerskaya sequence.

Many sedimentological characteristics of the Tulomozerskay magnesite–stromatolite–dolostone–'red bed' association are consistent with a restricted or partly restricted, evaporitic, oxidizing, stromatolite-dominated depositional environment. The presence of pseudomorphs after calcium sulphate and halite casts suggests that some of the TF sediments were deposited from a body of water whose composition was significantly different from that of seawater. Moreover, the dominance of highly oxidized 'red beds' in sequence is indicative of terrestrial rather than aqueous environments. Thus, the carbonate-depositing systems could have frequently been decoupled from the bordering sea. Therefore, such systems could hardly be maintained constantly in isotopic equilibrium with seawater. Consequently, we must inevitably conclude that there was a significant influence of local factors on the carbon isotope composition of the TF dolostones.

The $\delta^{13}C$ values plotted against the inferred depositional environments (Fig. 13) demonstrate that (1) the greatest enrichment in ^{13}C occurs in the playa magnesite (up to +17.2‰) and in the laminated stromatolites accreted in ephemeral ponds (up to +16.8‰), whereas (2) the

dolostones from more open environments are less rich in ^{13}C; some of them have values of +5 to +7‰ (Fig. 14). Although most of the dolostones accumulated in more open environments exhibit $\delta^{13}C$ ranging from +8 to +11‰, it is not yet clear to what extent these values might have been caused by incorporation (by current and tide activities) of dolostone clasts, which were initially accumulated in restricted settings. As is apparent from the histogram (Fig. 14), dolostones deposited in playa, sabkha, peritidal and lagoonal evaporitic environments are characterized by essentially the same $\delta^{13}C$ range, from +8 to +12‰. As these environments are supposedly partly or largely restricted, it is very unlikely that all the dolostones could have formed therein in isotopic equilibrium with seawater.

At this stage we are not able to quantify more precisely the roles of the global and local factors involved in the positive isotopic shift of $\delta^{13}C_{carb}$. A three-dimensional basinal model and comparison between distal (more open) and proximal (more restricted) facies combined with micro-core sampling would be required to answer some of these questions. Research into such a model has started recently, and hopefully its results will further illuminate the local and global factors causing the high ^{13}C enrichment in the TF carbonate rocks.

Conclusions

The Palaeoproterozoic TF is an 800 m-thick magnesite–stromatolite–dolostone–'red bed' sequence formed in a variety of settings, including a complex combination of shallow-marine and non-marine environments.

Terrigeneous 'red beds' developed throughout the sequence and exhibit great variation in thickness and lithofacies. The lowermost quartzitic sandstones (Members A and B) represent a braided fluvial system over a lower-energy, river-dominated coastal plain. Terrigenous 'red beds', forming the middle part of the sequence (Members A and C), are consistent with a low-energy, protected intertidal setting such as a barred lagoon or bight. The upper siliciclastic 'red beds' (Member E) were accumulated in a non-marine, playa lake environment under high-temperature, evaporitic conditions.

A significant part of the dolostones is biohermal and biostromal stromatolitic, formed in settings ranging from shallow-water, low-energy, intertidal through barred evaporitic lagoonal to peritidal evaporitic environments.

The flat-laminated stromatolitic dolostones were accreted in a restricted evaporative environment developed in either ephemeral ponds in peritidal zones or coastal sabkhas and playa lakes. The red coloration of the stromatolites indicates their frequent exposure to air.

The presence of tepees, mudcracks, pseudomorphs after calcium sulphate, halite casts, and abundant 'red beds' is indicative of the dominance of terrestrial rather than aqueous environments. Thus, the restricted or partly restricted stromatolite-dominated depositional systems could have been frequently decoupled from the bordering sea and subjected to various local factors such as evaporation, oxidation, and biological photosynthesis, which all might have caused an isotopic disequilibrium with seawater.

Only a small proportion of carbonates, developed in the middle part of Member B, at the base of Member D, and particularly in Member G, represent dolostones which accumulated in relatively 'open' environments.

The Tulomozerskaya dolostones and magnesite exhibit high $\delta^{13}C$ values ranging from +5.6 to +17.2‰. The greatest enrichment in ^{13}C occurs in the playa magnesite (up to +17.2‰) and in the laminated dolomitic stromatolites accreted in ephemeral ponds (up to +16.8‰), whereas the dolostones from more open environments are less rich in ^{13}C (+5.6 to +10.7‰).

The high $\delta^{13}C$ values were induced by a complex combination of a series of global and local factors. The global factor is the accelerated accumulation of organic material in an external basin(s). A global $\delta^{13}C$ value was locally superimposed by a series of local factors such as restriction, evaporation, and biological photosynthesis. The locally enhanced $\delta^{13}C$ values do not reflect the global shift, as they were generated in the local aquatic reservoirs, which were unlikely to be in isotopic equilibrium with atmospheric CO_2 and inorganic carbon dissolved in seawater.

The interaction between the global and local factors must be taken into account before full interpretation of the Palaeoproterozoic carbon isotope excursion and its implications can be made.

Acknowledgements. – This research was carried out by the Geological Survey of Norway (NGU) jointly with the Scottish Universities Environmental Research Centre (SUERC) (Glasgow, Scotland) and the Institute of Geology (IG) of the Russian Academy of Sciences (Petrozavodsk, Karelia). Access to core material of the Nevskaya and Karelian Geological Expeditions is acknowledged with thanks. The fieldwork was financially supported by Norsk Hydro. IG, and partly NGU and SUERC, were supported by INTAS-RFBR 095-928. D. Roberts read an earlier version of the manuscript and suggested improvements. The constructive criticism by the official referees, J. I. Fairchild, J. P. Nystuen, and M. R. Talbot, are appreciated.

Manuscript received May 1999

References

Adams, P. J. & Cowie, J. W. 1953: A geological reconnaissance of the region around the inner part of Danmarks Fjord, northeastern Greenland. *Meddelelser om Grønland 111(7),* 1–2.

Adams, J. E. & Frenzel, N. H. 1950: Capitan barrier reef, Texas and New Mexico. *Journal of Geology 58,* 289–312.

Akhmedov, A. M., Krupenik, V. A., Makarikhin, V. V. & Medvedev, P. V. 1993 *Carbon isotope composition of carbonates in the early Proterozoic sedimentary basins. Printed report, 58 pp. Institute of Geology of the Karelian Scientific Centre, Petrozavodsk,* in Russian.

Baker, A. J. & Fallick, A. E. 1989a: Evidence from Lewisian limestone for isotopically heavy carbon in two-thousand-million-year-old sea water. *Nature 337,* 352–354.

Baker, A. J. & Fallick, A. E. 1989b: Heavy carbon in two-billion-year-old marbles from Lofoten-Vesterålen, Norway: implications for the Precambrian carbon cycle. *Geochimica et Cosmochimica Acta 53,* 1111–1115.

Bathurst, R. G. C. 1976: Carbonate sediments and their diagenesis. Second

enlarged edition. *Developments in sedimentology 12, Elsevier, Amsterdam, Oxford, New York,* 658.

Beauchamp, B., Oldershaw, A. E. & Krouse, R. 1987: Upper Carboniferous to Upper Permian ^{13}C-enriched primary carbonates in the Sverdrup Basin, Canadian Arctic: comparisons to coeval western North American ocean margins. *Chemical Geology 65,* 391–413.

Bertrand-Sarafati, J. & Moussine-Pouchkine, A. 1985: Evolution and environmental conditions of the Conophyton associations in the Atar Dolomite (Upper Proterozoic), Mauritania. *Precambrian Research 29,* 207–234.

Bertrand-Sarafati, J. & Moussine-Pouchkine, A. 1988: Is cratonic sedimentation consistent with available models? An example from the Upper Proterozoic of the West African craton. *Precambrian Research 58,* 255–276.

Beukes, N. J. 1983: Palaeoenvironmental setting of iron-formation in the depositional basin of the Transvaal Supergroup, South Africa. *In* Trendall, A. F. & Morris, R. C. (eds.): *Iron Formations: Facts and Problems,* 131–209. Amsterdam, Elsevier.

Bonatti, C., Emiliani, C., Ostlund, G. & Rydel, H. 1971: Final desiccation of the Afar Rift, Ethiopia. *Science 172,* 468–469.

Burne, R. V. & James, N. 1986: Subtidal origin of club-shaped stromatolites, Shark Bay, W. A. *Australian Journal of Marine and Freshwater Resources 30,* 753–764.

Burne, R. V. & Moore, L. S. 1987: Microbiolites: organosedimentary deposits of benthic microbial communities. *Pallaios 2,* 241–254.

Bush, P. 1973: Some aspects of the diagenetic history of the Sabkha in Abu Dhabi, Persian Gulf. *In* Purser, B. H. (ed.): *The Persian Gulf,* 395–407. Springer-Verlag, New York.

Carpenter, S. J. & Lohman, K. C. 1997: Carbon isotope ratios of Phanerozoic marine cements: re-evaluation the global carbon and sulphur systems. *Geochimica et Cosmochimica Acta 61,* 4831–4846.

Castenholz, R. W., Bauld, J. & Pierson, B. K. 1992: Photosynthetic activity in modern microbial mat-building communities. *In* Schopf, J. W. & Klein, C. (eds.): *The Proterozoic Biosphere*, 279–285. Cambridge University Press.

Cohen, A. S., Talbot, M. R., Awramik, S. M., Dettman, D. L. & Abell, P. 1997: Lake level and paleoenvironmental history of Lake Tanganyka, Africa, as inferred from late Holocene and modern stromatolites. *Geological Society of America Bulletin 109,* 444–460.

Cohen, Y., Krumbein, W. E., Goldberg, M. & Shilo, M. 1977: Solar Lake (Sinai). 1. Physical and chemical limnology. *Limnology and Oceanography 22,* 597–608.

Coshell, L., Rosen, M. R. & McNamara, K. J. 1998: Hydromagnesite replacement of biomineralized aragonite in a new location of Holocene stromatolites, Lake Walyungup, Western Australia. *Sedimentology 45,* 1005–1018.

Curtis, R., Evans, G., Kinsman, D. J. J. & Shearman, D. J. 1963: Association of anhydrite and dolomite in the recent sediments of the Persian Gulf. *Nature 197,* 679–680.

Delaney, C. D. 1981: The Mid-Proterozoic Wernecke Supergroup, Wernecke Mountains, Yukon Territory. *Geological Survey of Canada Paper 81–10,* 1–23.

Demicco, R. V. & Hardie, L. A. 1994 *Sedimentary Structures and Early Diagenetic Features of Shallow Marine Carbonate Deposits, 265 pp. Society of Sedimentary Geology, Tulsa, Oklahoma, U.S.A.*

Dill, R. F., Shinn, E. A., Jones, A. T., Kelly, K. & Steinen, R. P. 1986: Giant subtidal stromatolites forming in normal salinity water. *Nature 324,* 55–58.

Fairchild, I. J. 1991: Origins of carbonate in Neoproterozoic stromatolites and the identification of modern analogues. *Precambrian Research 53,* 281–299.

Fairchild, I. J. & Hambrey, M. J. 1984: The Vendian succession of northeastern Spitsbergen: petrogenesis of a dolomite–tillite association. *Precambrian Research 26,* 111–167.

Fairchild, I. J. & Herrington, P. M. 1989: A tempestite–stromatolite–evaporite association (Late Vendian, East Greenland): a shoreface–lagoon model. *Precambrian Research 43,* 101–127.

Fairchild, I. J., Knoll, A. H. & Swett, K. 1991: Coastal lithofacies and biofacies associated with syndepositional dolomitization and silification (Drake Formation, Upper Riphean, Svalbard). *Precambrian Research 53,* 165–197.

Fairchild, I. J., Marshall, J. D. & Bertrand-Sarafati, J. 1990: Stratigraphic shift in carbon isotopes from Proterozoic stromatolitic carbonates (Mauritania): influence of primary mineralogy and diagenesis. *American Journal of Science 290-A,* 46–79.

Fairchild, I. J. & Spiro, B. 1987: Petrological and isotopic implications of some contrasting Late Precambrian carbonates, NE Spitsbergen. *Precambrian Research 34,* 973–989.

Ferguson, J., Burne, R. V. & Chambers, L. A. 1982: Lithification of peritidal carbonates by continental brines at Fisherman Bay, South Australia, to form a megapoligon/spelean limestone association. *Journal of Sedimentary Petrology 52,* 1127–1147.

Folk, R. L. 1962: Spectral subdivision of limestone types. *In* Ham, W. E. (ed.): *Classification of carbonate rocks*, 62–84. American Association of Petroleum Geologists Memoir 1.

Gebelin, C. D. 1969: Distribution, morphology and accretion rate of recent subtidal algal stromatolites, Bermuda. *Journal of Sedimentary Petrology 39,* 49–69.

Germs, G. J. B. 1983: Implications of a sedimentary facies and depositional environmental analysis of the Nama Group in South West Africa/Namibia. *Special Publications of the Geological Society of South Africa 11,* 89–114.

Goldhammer, R. K., Dunn, P. A. & Hardie, L. A. 1990: Depositional cycles, composite sea-level changes, cycle stacking patterns, and the hierarchy of stratigraphic forcing: Examples from Alpine Triassic platform carbonates. *Geological Society of America Bulletin 102,* 535–562.

Golubic, S. 1976: Organisms that build stromatolite. *In* Walter, M. R. (ed.): *Stromatolites*, 113–126. Elsevier Scientific Publishing Company, Amsterdam, Oxford, New York.

Golubic, S. 1985: Microbial mats and modern stromatolites in Shark Bay, Western Australia. *In* Caldwell, D. E., Brierley, J. A. & Brierley, C. L. (eds.): *Planetary Ecology*, 3–16. Van Nostrand Reinhold, New York.

Grotzinger, J. P. 1986: Evolution of Early Proterozoic passive-margin carbonate platform, Rocknest Formation, Wopmay Orogen, Northwest Territories, Canada. *Journal of Sedimentary Petrology 56,* 831–847.

Grotzinger, J. P. 1989: Facies and evolution of Precambrian carbonate depositional systems: emergence of the modern platform archetype. *In* Crevello, P. D., Wilson, J. L., Sarg, J. F. & Read, J. F. (eds.): *Controls on Carbonate Platform and Basin Developments.* Society of Economic Paleontologists and Mineralogists Special Publication 44, 79–106.

Grotzinger, J. P. & Read, J. F. 1983: Evidence for primary aragonite precipitation, lower Proterozoic (1.9 Ga) dolomite, Wopmay orogen, northwest Canada. *Geology 11,* 710–713.

Handford, C. F., Kendall, A. C., Prezbindowski, D. R., Dunham, J. B. & Logan, B. W. 1984: Salina-margin tepees, pisolites, and aragonite cements, Lake MacLeod, Western Australia: their significance in interpreting ancient analogs. *Geology* 12, 523–527.

Hardie, L. A., Bosellini, A. & Goldhammer, R. K. 1986: Repeated subaerial exposure of subtidal carbonate platforms, Triassic, northern Italy: evidence for high frequency sea level oscillations on a 10^4 year scale. *Paleoceanography 1,* 447–457.

Hardie, L. A., Lowenstein, T. K. & Spencer, R. J. 1985: The problem of distinguishing between primary and secondary features in evaporites. *In* Schreiber, B. C. (ed.): *Sixth International Symposium on Salt*, 11–93. Alexandria, Salt Institute.

Hardie, L. A. & Shinn, E. A. 1986: Carbonate depositional environments modern and ancient, part 3: tidal flats. *Colorado School of Mines Quarterly 81,* 1–74.

Heiskanen, K. I. 1990 *Palaeogeography of the Baltic Shield in Karelian Time, 124 pp. Karelian Science Centre, Petrozavodsk,* in Russian.

Hoffman, P. 1976: Environmental diversity of Middle Precambrian stromatolites. *In* Walter, M. R. (ed.): *Stromatolites*, 599–611. Elsevier Scientific Publishing Company, Amsterdam, Oxford, New York.

Hoffman, P. 1989: Pethey Reef complex (1.9 Ga). *In* Geldsetzer, H. H. J., James, N. P. & Tebbutt, G. E. (eds.): *Reefs: Canada and Adjacent Areas*, 38–48. Canadian Society of Petroleum Geologists Memoir 13.

ISSC (International Subcommission on Stratigraphic Classification of IUGS Commission on Stratigraphy) 1976 *In* Hedberg, H. D. (ed.): *International Stratigraphic Guide: A Guide to Stratigraphic Classification, Terminology and Procedure,* 1–200. John Wiley & Sons, New York.

James, N. P. 1984: Shallowing-upwards sequences in carbonates. *In* Walker, R. G. (ed.): *Facies Models*, 2nd edition. Geoscience Canada Reprint Series 1. St. Johns, Newfoundland, Geological Association of Canada, Toronto.

Jørgensen, B. B., Nelson, D. C. & Ward, D. M. 1992: Chemostratigraphy and decomposition in modern microbial mats. *In* Schopf, J. W. & Klein, C. (eds.): *The Proterozoic Biosphere*, 287–293. Cambridge University Press, Cambridge.

Kah, L. C. & Knoll, A. H. 1996: Microbenthid distribution of Proterozoic tidal flats: environmental and taphonomic considerations. *Geology 24,* 79–84.

Karhu, J. A. 1993: Palaeoproterozoic evolution of the carbon isotope ratios of sedimentary carbonates in the Fennoscandian Shield. *Geological Survey of Finland Bulletin 371,* 1–87.

Karhu, J. A. & Holland, H. D. 1996: Carbon isotopes and rise of atmospheric oxygen. *Geology 24,* 867–879.

Katz, A., Kolodny, Y. & Nissenbaum, A. 1977: The geochemical evolution of the Pleistocene Lake Lisisan–Dead Sea system. *Geochimica et Cosmochimica Acta 41,* 1609–1626.

Kendall, A. C. 1984: Evaporites. *In* Walker, R. G. (ed.): *Facies Models*, 2nd edition, 259–296. Geoscience Canada Reprint Series 1. St. Johns, Newfoundland, Geological Association of Canada, Toronto.

Kerans, C. & Donaldson, J. A. 1989: Deepwater conical stromatolite reef, Sulky Formation (Dismal Lake Group), Middle Proterozoic, N. W. T. *In* Geldsetzer, H. H. J., James, N. P. & Tebbutt, G. E. (eds.): *Reefs: Canada and Adjacent Areas*, 81–88. Canadian Society of Petroleum Geologists Memoir 13.

Kinsman, D. J. J. 1966: Gypsum and anhydrite of Recent age, Trucial Coast,

Persian Gulf. *In* Rau, J. L. (ed.): *Proceedings of the Second Salt Symposium 1*, 302–326. Cleveland, Northern Ohio Geological Society.

Knoll, A. H. & Swett, K. 1990: Carbonate deposition during the Late Proterozoic era: an example from Spitsbergen. *American Journal of Science 290-A,* 104–132.

Knoll, A. H., Swett, K. & Burkhardt, E. 1989: Paleoenvironmental distribution of microfossils and stromatolites from the Upper Proterozoic Backlundtoppen Formation, Spitsbergen. *Journal of Paleontology 63(2),* 129–145.

Krumbein, W. E., Cohen, Y. & Shilo, M. 1977: Solar Lake (Sinai). 4. Stromatolitic cyanobacterial mats. *Limnology and Oceanography 22,* 635–656.

Lindsay, J. F. 1987: Upper Proterozoic evaporites in the Amadeus Basin, central Australia, and their role in basin tectonics. *Geological Society of America Bulletin 99,* 852–865.

Logan, B. 1961: *Cryptozoon* and associated stromatolites from the Recent, Shark Bay, Western Australia. *Journal of Geology 69,* 517–533.

Magaritz, M., Anderson, R. Y., Holser, W. T., Saltzman, E. S. & Garber, J. 1983: Isotope shift in the Late Permian of the Delaware Basin, Texas, precisely timed by varved sediments. *Earth and Planetary Science Letters 66,* 111–124.

Makarikhin, V. V. & Kononova, G. M. 1983 *Early Proterozoic Phytolithes of Karelia, 180 pp. Nauka, Leningrad,* in Russian.

Masson, P. H. 1955: An occurrence of gypsum in southwest Texas. *Journal of Sedimentary Petrology 25,* 72–77.

McKenzie, J. A. 1981: Holocene dolomitisation of calcium carbonate sediments from coastal sabkhas of Abu Dhabi, U. A. E. – a stable isotope study. *Journal of Geology 89,* 185–198.

Melezhik, V. A. & Fallick, A. E. 1996: A widespread positive $\delta^{13}C_{carb}$ anomaly at around 2.33–2.06 Ga on the Fennoscandian Shield: a paradox? *Terra Nova 8,* 141–157.

Melezhik, V. A. & Fallick, A. E. 1997: Paradox regained? Reply. *Terra Nova 9,* 148–151.

Melezhik, V. A., Fallick, A. E., Makarikhin, V. V. & Lybtsov, V. V. 1997: Links between Palaeoproterozoic palaeogeography and rise and decline of stromatolites: Fennoscandian Shield. *Precambrian Research 82,* 311–348.

Melezhik, V. A., Fallick, A. E., Medvedev, P. V. & Makarikhin, V. V.: Extreme $^{13}C_{carb}$ enrichment in ca. 2.0 Ga magnesite–stromatolite–dolomite–'red beds' association in a global context: a case for the world-wide signal enhanced by a local environment. *Earth Science Reviews 48,* 71–120.

Melezhik, V. A., Fallick, A. E., Medvedev, P. V. & Makarikhin, V. V.: Palaeoproterozoic magnesite: lithological and isotopic evidence for playa/sabkha environments. *Sedimentology,* submitted.

Muir, M. D., Lock, D. & von der Borch, C. 1980: The Coorong model for penecontemporaneous dolomite formation in the Middle Proterozoic McArthur Group, Northern Territory, Australia. *Society Economic Paleontologists and Mineralogists Special Publication 28,* 51–67.

Montaggioni, L. F. & Camoin, G. F. 1993: Stromatolites associated with coralgal communities in Holocene high-energy reefs. *Geology 21,* 149–152.

Monty, C. L. V. 1976: The origin and development of cryptalgal structures. *In* Walter, M. R. (ed.): *Stromatolites*, 193–249. Elsevier Scientific Publishing Company, Amsterdam, Oxford, New York.

Negrutza, V. Z. 1984 *Early Proterozoic Development of the Eastern Part of the Baltic Shield, 270 pp. Nedra, Leningrad,* in Russian.

Pentecost, A. & Riding, R. 1986: Calcification of cyanobacteria. *In* Leadbeater, B. C. S. & Riding, R. (eds.): Biomineralization in Lower Plants and Animals, 73–90. Clarendon, Oxford.

Pierre, C. 1982 *Teneurs en isotopes stables (^{18}O, ^{2}H, ^{13}C, ^{34}S) et conditions de génèse des évaporites marines: application à quelques milieux actuels et au Messinian de la Méditerranée, D.S.N. Thesis, Université de Paris-Sud, Orsay,* 226.

Playford, P. E. 1990: Geology of the Shark Bay area, Western Australia. *In* Berry, P. F., Bradshaw, S. D. & Wilson, B. R. (eds.): Research in Shark Bay. Report of the France-Australe Bicentenary Expedition Committee, 13–31.

Playford, P. E. & Cockbain, A. E. 1976: Modern algal stromatolites at Hamelin Pool, a hypersaline barred basin in Shark Bay. *In* Walter, M. R. (ed.): *Stromatolites*, 389–411. Elsevier Scientific Publishing Company, Amsterdam, Oxford, New York.

Plumb, K., Derrick, G. M., Needham, R. S. & Shaw, R. D. 1981: The Proterozoic of Northern Australia. *In* Hunter, D. R. (ed.): Precambrian of the Southern Hemisphere, 205–307. Amsterdam, Elsevier.

Preiss, W. V., compiler. 1987: The Adelaide Geosyncline. *Geological Survey of South Australia Bulletin 53,* 1–438.

Pukhtel, I. S., Zhuravlev, D. Z., Ashikhmina, N. A., Kulikov, V. S. & Kulikova, V. V. 1992: Sm-Nd age of the Suisarskay suite on the Baltic Shield. *Transactions of the Russian Academy of Sciences 326,* 706–711 (in Russian).

Ricketts, B. D. & Donaldson, J. A. 1981: Sedimentary history of the Belcher Group of Hudson Bay. *Geological Survey of Canada Paper 81–10,* 235–254.

Rubin, D. M. & Friedman, G. M. 1977: Intermittently emergent shelf carbonates: an example from Cambro-Ordovician of eastern New York State. *Sedimentary Geology 19,* 81–106.

Schidlowski, M., Eichmann, R. & Junge, C. E. 1976: Carbon isotope geochemistry of the Precambrian Lomagundi carbonate province, Rhodesia. *Geochimica et Cosmochimica Acta 40,* 449–455.

Schroll, E. 1989: Recent formation of magnesite in evaporitic environment. The example of the Coorong Lagoon (South Australia). *In* Möller, P. (ed.): *Magnesite. Geology, Mineralogy, Geochemistry, Formation of Mg-Carbonates*, 29–34. *Monograph Series on Mineral Deposits 28.*.

Shearman, D. J. 1966: Origin of marine evaporites by diagenesis. *Transactions of the Institute of Mining and Metallurgy Section B 75,* 208–215.

Shields, G. 1997: A widespread positive $\delta^{13}C$ anomaly at around 2.33–2.06 Ga on the Fennoscandian Shields. Comment: paradox lost? *Terra Nova 9,* 148–151.

Shinn, E. A. 1983: Tidal flat environment. *In* Scholle, P. A., Bebout, D. G. & Moore, C. H. (eds.): *Carbonate Depositional Environments*, 173–210. Tulsa, American Association of Petroleum Geologists Memoir 33.

Siedlecka, A. 1976: Silicified Precambrian evaporite nodules from northern Norway: a preliminary report. *Sedimentary Geology 16,* 161–175.

Siedlecka, A. 1982: Supralittoral ponded algal stromatolites of the late Precambrian Annijokka Member of the Båtsfjord Formation, Varanger Peninsula, north Norway. *Precambrian Research 18,* 319–345.

Sochava, A. V. 1979 *Precambrian and Phanerozoic 'Red Beds', 207 pp. Nauka, Leningrad,* in Russian.

Sokolov, V. A. 1970 *Jatuli of Karelia and vicinities. D.Sc. Thesis, 52 pp. Geological Institute of the USSR Academy of Sciences, Moscow,* in Russian.

Sokolov, V. A. 1980: Jatulian formations of the Karelian ASSR. *In* Silvennoinen, A. (ed.): *Jatulian Geology in the Eastern Part of the Baltic Shield*, 163–220. Proceedings of a Finnish-Soviet Symposium held in Finland, 21–26 August 1979. Rovaniemi. The Committee for Scientific and Technical Cooperation between Finland and Soviet Union.

Sokolov, V. A. 1987: The Jatulian Superhorizon. *In* Sokolov, V. A. (ed.): *The Geology of Karelia*, 51–59. Nauka, Leningrad, in Russian.

Sokolov, V. A., Galdobina, L. P., Ryleev, A. B., Catzuk, Yu. I. & Kheskanen, K. I. 1970 *Geology, sedimentology and palaeogeography of the Jatuli, Central Karelia, 363 pp. Institute of Geology, Karelian Science Centre, Petrozavodsk, Russia,* in Russian.

Southgate, P. N. 1986: Depositional environment and mechanism of preservation of microfossils, upper Proterozoic Bitter Springs Formation, Australia. *Geology 14,* 683–686.

Southgate, P. N. 1989: Relationship between cyclicity and stromatolite form in the Late Proterozoic Bitter Springs Formation, Australia. *Sedimentology 36,* 323–339.

Spencer, R. J. & Lowenstein, T. K. 1990: Evaporites. *In* McIlreath, I. A. & Morrow, D. W. (eds.): *Diagenesis*, 141–146. Geoscience Canada Reprint Series 4. St. Johns, Newfoundland, Geological Association of Canada, Toronto.

Stiller, M., Rounick, J. S. & Shasha, S. 1985: Extreme carbon-isotope enrichments in evaporitic brines. *Nature 316,* 434–435.

Tappan, H. 1968: Primary production, isotopes, extinctions and the atmosphere. *Paleogeography Paleoceanography Paleoecology 4,* 187–210.

Tucker, M. E. 1976: Replaced evaporites from the late Precambrian of Finnmark, Arctic Norway. *Sedimentary Geology 16,* 193–204.

Tucker, M. E. 1982: Precambrian dolomites: petrographic and isotopic evidence that they differ from Phanerozoic dolomites. *Geology 10,* 7–12.

Tucker, M. E. 1983a: Sedimentation of organic-rich limestones in the late Precambrian of southern Norway. *Precambrian Research 22,* 295–315.

Tucker, M. E. 1983b: Diagenesis, geochemistry, and origin of a Precambrian dolomite: the Beck Spring Dolomite of eastern California. *Journal of Sedimentary Petrology 53,* 1097–1119.

Tucker, M. E. & Wright, V. P. 1990 *Carbonate Sedimentology, 482 pp. Oxford.*

Walter, M. R. (ed.) 1976 *Stromatolites, 790 pp. Elsevier Scientific Publishing Company, Amsterdam, Oxford, New York.*

Walter, M. R., Golubic, S. & Preiss, W. V. 1973: Recent stromatolites from hydromagnesite and aragonite depositing lakes near Coorong Lagoon, South Australia. *Journal of Sedimentary Petrology 43,* 10021–11030.

Yudovich, Ya. E., Makarikhin, V. V., Medvedev, P. V. & Sukhanov, N. V. 1991: Carbon isotope anomalies in carbonates of the Karelian Complex. *Geochemical International 28(2),* 56–62.

Zempolich, W. G., Wilkinson, B. H. & Lohman, K. C. 1988: Diagenesis of Late Proterozoic carbonates: the Beck Spring Dolomite of eastern California. *Journal of Sedimentary Petrology 58,* 656–672.